arXiv:1110.6359v2 [cond-mat.mes-hall] 20 Jan 2012

Coulomb drag in graphene: perturbation theory

B.N. Narozhny,[1] M. Titov,[2,3] I.V. Gornyi,[3,4] and P.M. Ostrovsky[3,5]

[1]*Institut für Theorie der Kondensierten Materie and DFG Center for Functional Nanostructures, Karlsruher Institut für Technologie, 76128 Karlsruhe, Germany*
[2]*School of Engineering & Physical Sciences, Heriot-Watt University, Edinburgh EH14 4AS, UK*
[3]*Institut für Nanotechnologie, Karlsruhe Institute of Technology, D-76021 Karlsruhe, Germany*
[4]*A.F. Ioffe Physico-Technical Institute, 194021 St. Petersburg, Russia*
[5]*L.D. Landau Institute for Theoretical Physics RAS, 119334 Moscow, Russia*

(Dated: January 23, 2012)

We study the effect of Coulomb drag between two closely positioned graphene monolayers. In the limit of weak electron-electron interaction and small inter-layer spacing ($\mu_{1(2)}, T \ll v/d$) the drag is described by a universal function of the chemical potentials of the layers $\mu_{1(2)}$ measured in the units of temperature T. When both layers are tuned close to the Dirac point, then the drag coefficient is proportional to the product of the chemical potentials $\rho_D \propto \mu_1\mu_2$. In the opposite limit of low temperature the drag is inversely proportional to both chemical potentials $\rho_D \propto T^2/(\mu_1\mu_2)$. In the mixed case where the chemical potentials of the two layers belong to the opposite limits $\mu_1 \ll T \ll \mu_2$ we find $\rho_D \propto \mu_1/\mu_2$. For stronger interaction and larger values of d the drag coefficient acquires logarithmic corrections and can no longer be described by a power law. Further logarithmic corrections are due to the energy dependence of the impurity scattering time in graphene (for $\mu_{1(2)} \gg T$ these are small and may be neglected). In the case of strongly doped (or gated) graphene $\mu_{1(2)} \gg v/d \gg T$ the drag coefficient acquires additional dependence on the inter-layer spacing and we recover the usual Fermi-liquid result if the screening length is smaller than d.

PACS numbers: 72.80.Vp, 73.23.Ad, 73.63.Bd

Transport measurements are conceptually simplest and by far the most common experimental tools for studying inner workings of solids. Within linear response, the outcome of such measurements is determined by the properties of the unperturbed system, which are often the object of study. In a typical experiment a current is driven through a conductor and the voltage drop along the conductor is measured. In most conventional conductors at low temperatures the resulting resistance is mostly determined by disorder (which is always present in any sample), while interactions between charge carriers lead to corrections that affect the temperature dependence[1].

Consider now a drag measurement in a bi-layer system consisting of two closely spaced but electrically isolated conductors[2]. Passing a current I_1 through one of these conductors ("the active layer") is known to induce a voltage V_2 in the other conductor ("the passive layer"). The ratio of this voltage to the driving current $\rho_D = -V_2/I_1$ (the transresistivity or the drag coefficient) is a measure of inter-layer interaction. At low enough temperatures the drag is dominated by the direct Coulomb interaction between charge carriers in both layers[2].

The physics of the Coulomb drag is well understood if both layers are in the Fermi liquid state[3,4]. The current in the passive layer is created by exciting electron-hole pairs (each pair consisting of an occupied state above the Fermi surface and an empty state below) in a state characterized by finite momentum. The momentum comes from the electron-hole excitations in the active layer created by the driving current. The momentum transfer is due to the inter-layer Coulomb interaction. Therefore it follows from the usual phase-space considerations that the drag coefficient is proportional to the square of the temperature $\rho_D \propto T^2$. Remarkably, this simple argument is sufficient to describe the observed temperature dependence of ρ_D (deviations from the quadratic dependence are due to the effect of phonons)[2].

The phase-space argument however does not describe the physics of the effect completely. Indeed, in the passive layer the momentum is transferred equally to electrons and holes so that the resulting state can carry current only in the case of electron-hole asymmetry. Likewise, this asymmetry is necessary for the current-carrying state in the active layer to be characterized by nonzero total momentum. In the Fermi-liquid theory the electron-hole asymmetry can be expressed[5] (assuming either a constant impurity scattering time or diffusive transport[6]) as a derivative of the single-layer conductivity $\sigma_{1(2)}$ with respect to the chemical potential. In conventional semiconductors[3] the asymmetry appears due to curvature of the conduction band spectrum (leading to the energy dependence of the density of states (DoS) and/or diffusion coefficient): $\partial\sigma_i/\partial\mu_i \approx \sigma_i/\mu_i$.

Theoretical calculations[2,3] typically focus on the drag conductivity σ_D. The experimentally measurable drag coefficient ρ_D is then obtained by inverting the 2×2 conductivity matrix. To the lowest order in the inter-layer interaction[3] (assuming $\sigma_D \ll \sigma_{1(2)}$) one obtains

$$\rho_D = \sigma_D/(\sigma_1\sigma_2). \tag{1}$$

Combining the above arguments (and assuming that the single-layer conductivities σ_i are given by the Drude formula) we arrive at the Fermi-liquid result[3]

$$\rho_D = \frac{\hbar}{e^2}\frac{T^2}{\mu_1\mu_2}A_{12}, \tag{2}$$

where A_{12} depends on the matrix elements of the inter-layer interaction, the Fermi momenta of the two layers, and the inter-layer spacing d (in the diffusive regime, where the mean-free path $\ell \ll d$, A_{12} contains an additional logarithmic dependence[3]). The precise form of A_{12} is well known and can be obtained by means of either the diagrammatic formalism[3] or the kinetic equation[7,8].

Recently drag measurements were performed in a system of two parallel graphene sheets[9]. It was shown that this system offers much greater flexibility compared to prior experiments in semiconductor heterostructures[10]. The drag coefficient depends on the following parameters: (i) temperature T, (ii) chemical potentials of the layers μ_i, (iii) inter-layer spacing d, (iv) mean-free path ℓ_i, and (v) the interaction strength. Earlier experiments[10] were performed on samples with large inter-layer spacing, such that $\mu \gg v/d$ (where v is the Fermi velocity). In contrast, the graphene-based system allows one to scan a wide range of chemical potentials (by electrostatically controlling carrier density) from the Fermi-liquid regime with $\mu_i \gg v/d, T$ to the Dirac point $\mu = 0$ where the drag vanishes due to electron-hole symmetry.

Most experiments[2,10] (including that of Ref. 9) are performed in the ballistic regime $\ell_i \gg d$, where ρ_D does not explicitly depend on disorder, albeit the conductivities σ_D and σ_i do. The graphene-based sample of Ref. 9 is characterized by much smaller inter-layer spacing in comparison to previous experiments[2], with all data taken at

$$T < v/d. \tag{3}$$

Therefore in this paper we do not consider temperatures larger than the inverse inter-layer spacing, even though our approach remains valid for $T \gtrsim v/d$.

In this paper we address the problem of the Coulomb drag in graphene by means of the perturbation theory. In the leading order, i.e. in the limit of weak interaction

$$\alpha = e^2/v \ll 1, \tag{4}$$

the drag conductivity σ_D is described by the standard (Aslamazov-Larkin-type, see Fig. 1) diagram[3]. Unlike usual metals, the single-layer conductivity in graphene comprises two competing contributions: one due to disorder and one due to electron-electron interaction[11–14]. We assume that the dominant scattering mechanism is due to disorder. Hence throughout the paper we assume

$$\alpha^2 T\tau \ll 1 \ll T\tau, \tag{5}$$

where τ is the impurity scattering time (in the case of energy-dependent impurity scattering time this parameter should be understood as $\tau(\max[\mu, T])$, see Sec. IV B). The latter inequality ensures that the system is in the ballistic regime. Under this condition[14] the single-layer conductivities $\sigma_{1(2)}$ are again given by the Drude-like formula with the impurity scattering time. As we will show, $\sigma_D/\sigma_{1(2)} \lesssim \alpha^2 T\tau \ll 1$, which allows us to evaluate the drag coefficient ρ_D using Eq. (1). Our theory can be further extended to the case of stronger interaction or vanishing disorder, where the condition (5) can be lifted. However it is more convenient to perform such calculations within the framework of the kinetic equation[11,12]. The results of that work are reported elsewhere[15].

TABLE I: Asymptotic expressions for the drag coefficient (6) in the limit of weak inter-layer interaction and small inter-layer spacing $\mu_{1(2)}, T \ll v/d$.

parameter region	drag coefficient	
$\mu_1, \mu_2 \ll T$	$\rho_D \approx 1.41\ \alpha^2 \frac{\hbar}{e^2} \frac{\mu_1\mu_2}{T^2}$	Eq.(35)
$\mu_1 \ll T \ll \mu_2$	$\rho_D \approx 5.8\ \alpha^2 \frac{\hbar}{e^2} \frac{\mu_1}{\mu_2}$	Eq.(36)
$T \ll \mu_1 < \mu_2$	$\rho_D \approx \alpha^2 \frac{\hbar}{e^2} \frac{8\pi^2}{3} \frac{T^2}{\mu_1\mu_2} \ln\frac{\mu_1}{T}$	Eq.(37)

In the limit of small inter-layer spacing $\mu_{1(2)}, T \ll v/d$ the resulting drag coefficient is the "universal" function

$$\rho_D = \alpha^2 \frac{\hbar}{e^2}\, r_0(\mu_1/T, \mu_2/T). \tag{6}$$

The function $r_0(x_1, x_2)$ is characterized by the limiting cases $\mu_i \ll T$ and $\mu_i \gg T$, see Table I. In the vicinity of the Dirac point $\rho_D \propto \mu_1\mu_2/T^2$, while in the opposite limit $\rho_D \propto T^2/(\mu_1\mu_2)$ (with additional logarithmic factors, see Sec. III). In the "mixed" case $\mu_1 \ll T \ll \mu_2$ we find $\rho_D \propto \mu_1/\mu_2$. This regime is apparently realized in the experiment of Ref. 9 when the bottom layer is in proximity of the Dirac point.

For relatively large inter-layer spacing, $\mu_i \gg v/d$ (and thus $\mu_i \gg T$), a new regime appears, where the drag coefficient acquires additional dependence on the inter-layer spacing. Here the assumption (4) may be relaxed as the perturbation theory remains valid also for intermediate values of α (see Sec. IV A where we assume $\mu_1 = \mu_2$). Still, for $\mu \ll T$ we find $\rho_D \propto \mu^2/T^2$, at $\mu \sim T$ the drag coefficient reaches its maximum, and further decays for $\mu \gg T$. The latter regime is described by a long crossover from the above logarithmic behavior to the Fermi-liquid result which is only achieved in the limit of the small screening length $\varkappa d \gg 1$. Thus $\rho_D(\mu \gtrsim v/d)$ cannot be described by a single power law.

The remainder of this paper is organized as follows. In Sec. I we present the perturbative calculation that gives the drag resistivity in the limit $\alpha \to 0$ and $d \to 0$. While the resulting expression can only be evaluated numerically, we analyze all interesting limits analytically for the case of two identical layers in Sec. II and also for the experimentally relevant case where the two layers are characterized by different chemical potentials, see Sec. III. In Sec. IV we discuss drag at intermediate values of α and d as well as the role of energy-dependent scattering time. The paper is concluded by a brief summary and a discussion of the experimental relevance of our results. Throughout the paper we use the units with $\hbar = 1$ and only restore the Planck's constant in the results for ρ_D. Technical details are relegated to Appendices.

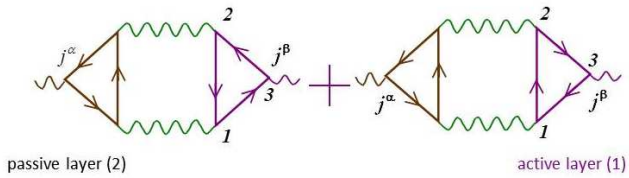

FIG. 1: [Color online] The lowest-order diagram for drag conductivity. Solid lines represent the exact single-electrons Green's functions in the presence of disorder. Spatial coordinates are labeled by the numbers shown at the corners of the triangles and correspond to the subscripts in Eq. (13). Wavy lines represent the inter-layer interaction.

I. PERTURBATIVE CALCULATION OF THE COULOMB DRAG

Consider the limit of weak interaction $\alpha \to 0$. In this case the drag conductivity σ_D can be calculated with the help of the lowest-order diagram[3]

$$\sigma_D^{\alpha\beta} = \frac{1}{16\pi T}\sum_{\boldsymbol{q}}\int \frac{d\omega}{\sinh^2\frac{\omega}{2T}}\Gamma_1^\beta(\omega,\boldsymbol{q})\Gamma_2^\alpha(\omega,\boldsymbol{q})|\mathcal{D}_{12}^R|^2, \tag{7}$$

where the subscripts 1 and 2 refer to the active and passive layers respectively, $\mathcal{D}_{12}^R$ is the retarded propagator of the inter-layer interaction, and $\Gamma_a^\alpha(\omega,\boldsymbol{q})$ is the non-linear susceptibility (or the rectification coefficient).

A. Inter-layer interaction for small α and d

The bare Coulomb potential has the usual form

$$V_{11} = V_{22} = \frac{2\pi e^2}{q}; \quad V_{12} = \frac{2\pi e^2}{q}\, e^{-qd}. \tag{8}$$

The dynamically screened (within RPA) inter-layer propagator can be written as[16]

$$\mathcal{D}_{12}^R = -\frac{1}{\Pi_1^R\Pi_2^R\frac{4\pi e^2}{q}\sinh qd + \left(\frac{q}{2\pi e^2}+\Pi_1^R+\Pi_2^R\right)e^{qd}}, \tag{9}$$

where Π_i^R is the single-layer retarded polarization operator. For $\alpha \ll 1$ screening is ineffective and the inter-layer interaction is essentially unscreened. Moreover, in the limit $d \to 0$ we may disregard the exponential and write the interaction propagator as

$$\mathcal{D}_{12}^R = -\frac{2\pi e^2}{q}. \tag{10}$$

As we will show below, the non-linear susceptibility $\boldsymbol{\Gamma}$ decays exponentially for $q \gg \max(T,\mu)$. Therefore, in view of Eq. (3) the limit $d \to 0$ is equivalent to the condition $\mu \ll v/d$ (the case $\mu_i > v/d$ is discussed in Sec. IV A).

B. Non-linear susceptibility in graphene

The non-linear susceptibility of electrons $\Gamma_{ij}^\alpha(\omega)$ is a response function relating a voltage $V(r_i)e^{i\omega t}$ to a *dc* current it induces by the quadratic response:

$$\mathbf{I} = \int d\boldsymbol{r}_1 \int d\boldsymbol{r}_2 \boldsymbol{\Gamma}(\omega;\boldsymbol{r}_1,\boldsymbol{r}_2)V(\boldsymbol{r}_1)V(\boldsymbol{r}_2), \tag{11}$$

with $\mathbf{I}$ being the induced *dc* current. From gauge invariance it follows that

$$\int d\boldsymbol{r}_1 \boldsymbol{\Gamma}(\omega;\boldsymbol{r}_1,\boldsymbol{r}_2) = \int d\boldsymbol{r}_2 \boldsymbol{\Gamma}(\omega;\boldsymbol{r}_1,\boldsymbol{r}_2) = 0.$$

In terms of exact Green's functions of a disordered conductor the non-linear susceptibility can be written as[3,17]

$$\boldsymbol{\Gamma} = \int \frac{d\epsilon}{2\pi}\Bigg[\left(\tanh\frac{\epsilon-\mu}{2T} - \tanh\frac{\epsilon+\omega-\mu}{2T}\right)\boldsymbol{\gamma}_{12}(\epsilon;\omega) + \left(\tanh\frac{\epsilon-\mu}{2T} - \tanh\frac{\epsilon-\omega-\mu}{2T}\right)\boldsymbol{\gamma}_{21}(\epsilon;-\omega)\Bigg], \tag{12}$$

where the arguments of $\boldsymbol{\Gamma}$ are suppressed for brevity, the subscripts 1 and 2 refer to the spatial coordinates $\boldsymbol{r}_1$ and $\boldsymbol{r}_2$, respectively, and the triangular vertex $\boldsymbol{\gamma}$ is given by

$$\boldsymbol{\gamma}_{12}(\epsilon;\omega) = \left[G_{12}^R(\epsilon+\omega) - G_{12}^A(\epsilon+\omega)\right]G_{23}^R(\epsilon)\,\hat{\mathbf{J}}_3 G_{31}^A(\epsilon). \tag{13}$$

Here $\hat{\mathbf{J}}_3$ is the current operator and integration over the coordinate $\boldsymbol{r}_3$ is assumed (see Fig. 1).

The traditional approach calls for averaging the vertex $\boldsymbol{\gamma}$ over disorder. Within the Fermi-liquid theory the averaged $\boldsymbol{\gamma}$ does not depend on ϵ[1,3]. This result is based on the usual approximation that the most important contribution comes from electrons near the Fermi surface. In contrast, in graphene-based systems the regime where the chemical potential is smaller that temperature $\mu_i \ll T$ is accessible. Then the vertex $\boldsymbol{\gamma}$ retains its dependence on ϵ and should be evaluated with care[18–20]. Details of the calculation are provided in Appendices A and B. The result is

$$\boldsymbol{\gamma}(\epsilon,\omega,q) = -2\boldsymbol{q}ev\tau(\epsilon)\frac{\omega^2+2\epsilon\omega-v^2q^2}{\epsilon v^2q^2} \times\sqrt{\frac{[2\epsilon+\omega]^2-v^2q^2}{v^2q^2-\omega^2}}\,\mathrm{sgn}(\epsilon+\omega)\theta_0(\epsilon,\omega,q), \tag{14}$$

where the function $\theta_0(\epsilon,\omega,q)$ ensures that the expression under the square root in Eq. (14) is always positive (the minus signs in $\theta_0(\epsilon,\omega,q)$ reflect the contribution of both electrons and holes and appear after summing over all branches of the Dirac spectrum in graphene)

$$\theta_0(\epsilon,\omega,q)=\theta(vq-|2\epsilon+\omega|)\left[\theta(-\omega-vq)-\theta(\omega-vq)\right]+\theta(vq-|\omega|)\left[\theta(2\epsilon+\omega-vq)-\theta(-vq-2\epsilon-\omega)\right]. \quad (15)$$

Approximating[21] the impurity scattering time by a constant τ (the effect of energy-dependent $\tau(\epsilon)$ is discussed below in Sec. IV B), we can express the non-linear susceptibility in terms of dimensionless variables

$$W=\frac{\omega}{2T},\quad Q=\frac{vq}{2T},$$

and find the following form

$$\mathbf{\Gamma}(\omega,\boldsymbol{q})=-2\frac{e\tau}{\pi}\,\boldsymbol{q}\,g\left(W,Q;\frac{\mu}{T}\right), \quad (16a)$$

$$g\left(W,Q;x\right)=\begin{cases}\sqrt{\frac{W^2}{Q^2}-1}\int\limits_0^1 dz\frac{z\sqrt{1-z^2}}{z^2-W^2/Q^2}\,I_2(z;W,Q;x), & |W|>Q\\ -\sqrt{1-\frac{W^2}{Q^2}}\int\limits_1^\infty dz\,\frac{z\sqrt{z^2-1}}{z^2-W^2/Q^2}\,I(z;W,Q;x), & |W|<Q\end{cases} \quad (16b)$$

$$I(z;W,Q;x)=\tanh\frac{zQ+W+x}{2}-\tanh\frac{zQ+W-x}{2}+\tanh\frac{zQ-W-x}{2}-\tanh\frac{zQ-W+x}{2}. \quad (16c)$$

From Eq. (16c) it is clear that at the Dirac point the non-linear susceptibility vanishes:

$$I(x=0)=0\;\Rightarrow\;\mathbf{\Gamma}(\mu=0)=0. \quad (17)$$

Thus there is no drag at the Dirac point (physically, due to electron-hole symmetry).

C. Perturbative results for the Coulomb drag in graphene

1. Drag conductivity in graphene

Using Eqs. (10) and (16) we can find the drag conductivity in graphene (7). As usual for an isotropic system in the absence of external magnetic fields $\sigma_D^{\alpha\beta}=\delta^{\alpha\beta}\sigma_D$. Now, in the limit $\alpha\to 0$ and $d\to 0$ we find

$$\sigma_D=\alpha^2e^2T^2\tau^2f_0\left(\frac{\mu_1}{T},\frac{\mu_2}{T}\right), \quad (18a)$$

where the dimensionless function $f_0(x_1,x_2)$ is defined as

$$f_0(x_1,x_2)=\frac{4}{\pi^2}\int\limits_0^\infty QdQ\int\limits_0^\infty\frac{dW}{\sinh^2 W}\,g(x_1)g(x_2). \quad (18b)$$

where we have suppressed the arguments of the function $g\left(W,Q;x\right)$ for brevity.

In general the function $f_0(x_1,x_2)$ has to be computed numerically. Below, we evaluate this function analytically in the physically interesting limiting cases of large x (the low temperature regime) and small x (the vicinity of the Dirac point).

2. Single-layer conductivity in graphene

In order to find the drag coefficient ρ_D one needs to know the single-layer conductivity σ_i. Under our assumptions the single-layer conductivity is completely determined by the weak impurity scattering and can be written in the form

$$\sigma_0=e^2T\tau h_0\left(\frac{\mu}{T}\right), \quad (19)$$

where

$$h_0(x)=\frac{2}{\pi}\int\limits_{-\infty}^{\infty}dz\frac{|z|}{\cosh^2\left(z+\frac{x}{2}\right)}=\frac{2}{\pi}\begin{cases}x, & x\gg 1,\\ 2\ln 2, & x\ll 1.\end{cases} \quad (20)$$

3. The drag coefficient

Finally, using Eqs. (1), (18a), and (19) we find that the drag coefficient can indeed be expressed in the form (6), with the dimensionless function $r_0(x_1,x_2)$ defined as

$$r_0(x_1,x_2)=\frac{f_0(x_1,x_2)}{h_0(x_1)h_0(x_2)} \quad (21)$$

In the case of two identical layers this function depends on one variable only

$$r_0(x)=\frac{f_0(x,x)}{h_0^2(x)},$$

and is shown in Fig. 2.

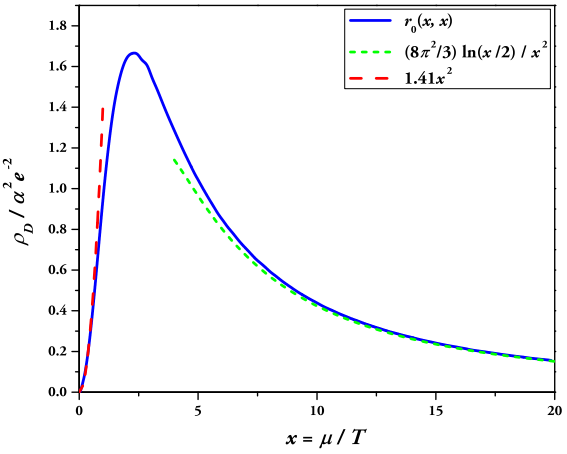

FIG. 2: [Color online] The dimensionless drag coefficient $r_0(x,x)$ (two identical layers). The solid line shows the result of numerical evaluation using Eqs. (21), (20), (18b), and (16). The red dashed line shows the asymptotic behavior (27) in the vicinity of the Dirac point. The green short-dashed line shows the asymptotic behavior (33) at small temperatures.

The expressions (6) and (21) give the perturbative result for the drag coefficient in graphene-based bi-layer systems in terms of the dimensionless functions $h_0(x)$ and $f_0(x_1,x_2)$. The applicability of this "universal" result and its experimental relevance is discussed in Sec. IV.

II. ASYMPTOTIC BEHAVIOR OF THE DRAG BETWEEN TWO IDENTICAL LAYERS

Consider now the case where the two layers in the drag experiment are identical, i.e. are kept at the same temperature and chemical potential. This case has not been yet realized experimentally in graphene-based systems, but has a long history of theoretical research[2,3].

A. Vicinity of the Dirac point

We start with situation where the graphene sheets are tuned close to the Dirac point, i.e.

$$\mu \ll T.$$

Given that at the Dirac point the nonlinear susceptibility vanishes [see Eq. (17)], we can expand it to the lowest order in the small parameter μ/T. Expanding first the expression (16c) we find

$$I(x\to 0) \approx -4x\frac{\sinh W \sinh zQ}{(\cosh zQ+\cosh W)^2}. \tag{22}$$

This corresponds to the quadratic expansion of Eq. (18b)

$$f_0(x,x) \approx \mathcal{N}_1 x^2. \tag{23}$$

The numerical coefficient $\mathcal{N}_1$ can now be determined by using the approximation (22) in Eqs. (16b) and (16b) and then evaluating the integral in Eq. (18b). The result is

$$\mathcal{N}_1 \approx 1.1. \tag{24}$$

Therefore the drag conductivity in the vicinity of the Dirac point is independent of temperature and is proportional to the square of the chemical potential

$$\sigma_D(\mu \ll T) \approx \alpha^2 e^2 \mu^2 \tau^2 \mathcal{N}_1. \tag{25}$$

In this case the drag conductivity is independent of T.

The single-layer conductivity can be found by expanding the function $h_0(x)$. Thus in the vicinity of the Dirac point the conductivity of a single graphene sheet due to impurity scattering [see Eq. (5)] is[14]

$$\sigma_0 \approx \frac{4\ln 2}{\pi}\, e^2 T\tau. \tag{26}$$

Therefore the drag coefficient is

$$\rho_D(\mu \ll T) \approx \alpha^2 \frac{\hbar}{e^2}\frac{\pi^2\mathcal{N}_1}{16\ln^2 2}\frac{\mu^2}{T^2} = 1.41\alpha^2\frac{\hbar}{e^2}\frac{\mu^2}{T^2}. \tag{27}$$

This result is represented in Fig. 2 by the dashed red line.

B. Low temperature limit

In the opposite limit

$$\mu \gg T$$

we notice that the function I_2 is given by Eq. (22) with interchanged W and x and can be written as

$$I(x\gg 1) \approx \frac{4W}{Q}\frac{\partial}{\partial z}\frac{\sinh x}{\cosh zQ+\cosh x}. \tag{28}$$

Then the integral over z in Eq. (16b) is dominated by $z \gg 1$ so that the algebraic function of z in the integrand may be approximated by unity. The corresponding contribution (16b) to the non-linear susceptibility may now be approximated by the expression[23]

$$g(x,|W|<Q) = 4\frac{W}{Q}\sqrt{1-\frac{W^2}{Q^2}}\frac{\sinh x}{\cosh Q+\cosh x}. \tag{29}$$

Now the momentum integral in Eq. (18b) is logarithmic and is dominated by large values of momentum $Q \gg W$. Then the function (18b) takes the form

$$f_0(x,x) = \frac{64}{\pi^2}\int_0^\infty \frac{dW W^2}{\sinh^2 W}\int_W^\infty \frac{dQ}{Q}\frac{\sinh^2 x}{(\cosh Q+\cosh x)^2}. \tag{30}$$

The ratio of the hyperbolic functions in Eq. (30) is similar to the step function: it's equal to unity for $Q \ll x$ and vanishes at larger values of momentum $Q \gg x$. Therefore

x effectively acts as the upper cut-off and the momentum integral can be approximated by a logarithm

$$\int\limits_W^\infty \frac{dQ}{Q} \frac{\sinh^2 x}{(\cosh Q + \cosh x)^2} \approx \ln \frac{x}{W}.$$

Therefore, in the low temperature limit the leading contribution to the drag conductivity is logarithmic in the chemical potential and quadratic in temperature

$$\sigma_D(T \ll \mu) \approx \frac{32}{3}\, \alpha^2 e^2 T^2 \tau^2 \ln \frac{\mu}{T}. \tag{31}$$

The single-layer conductivity at low temperatures is determined by the chemical potential[14] and thus is given by the Drude formula

$$\sigma_0 \approx (2/\pi)\, e^2 \mu \tau. \tag{32}$$

Consequently the drag coefficient is similar to Eq. (2).

$$\rho_D(\mu \gg T) \approx \alpha^2 \frac{\hbar}{e^2} \frac{8\pi^2}{3} \frac{T^2}{\mu^2} \ln \frac{\mu}{T}. \tag{33}$$

This is to be expected, since at low temperatures $T \ll \mu$ the phase-space argument yielding the T^2 dependence is justified and the electron-hole asymmetry determines the dependence on the chemical potential. The logarithmic factor is of course beyond such qualitative estimates.

This result (33) is represented in Fig. 2 by the dashed green line and is shown together with the result of the direct numerical calculation (shown by the solid blue line). Note that the drag conductivity (31) was calculated with logarithmic accuracy.

III. ASYMPTOTIC BEHAVIOR OF THE DRAG BETWEEN INEQUIVALENT LAYERS

Consider now the more realistic[9] situation where the two layers are characterized by different chemical potentials. We will still assume that the temperatures of the two layers are the same.

Note that in this Section the subscripts of the chemical potentials μ_1 and μ_2 do not indicate the passive and active layers, but rather simply distinguish between two layers with different carrier density.

A. One layer near the Dirac point

Firstly, suppose that one of the two layers is characterized by a small chemical potential

$$\mu_1 \ll T.$$

Then in Eq. (18b) the function $g(x_1)$ may be expanded using Eq. (22):

$$\sigma_D = \alpha^2 e^2 \mu_1 T \tau^2 f_1\left(\frac{\mu_2}{T}\right).$$

The dimensionless function $f_1(x)$ is characterized by the two limits. If the second layer is also close to the Dirac point, then

$$f_1(x \ll 1) \approx \mathcal{N}_1 x,$$

which yields a straightforward generalization of Eq. (23): $f_0(x_1, x_2) \approx \mathcal{N}_1 x_1 x_2$. If, on the other hand the chemical potential of the second layer is large compared to T, then the drag conductivity (18b) can be calculated by using the linear approximation (22) for $g(x_1)$ and the low temperature approximation (29) for $g(x_2)$. Due to the exponential decay of Eq. (22) at $Q \gg W$, the momentum integral is dominated by $Q \sim 1$ and thus the combination of the hyperbolic functions in Eq. (29) can be replaced by unity. Thus in this limit the drag conductivity in independent of the chemical potential of the second layer and

$$f_1(x \gg 1) \approx \mathcal{N}_2, \quad \mathcal{N}_2 \approx 3.26. \tag{34}$$

Now, the single-layer conductivity in the first layer is given by Eq. (26), while in the second layer we should consider both limits. If μ_2 is also small then the resulting drag coefficient is a trivial generalization of Eq. (27):

$$\rho_D(\mu_1, \mu_2 \ll T) \approx 1.41 \alpha^2 \frac{\hbar}{e^2} \frac{\mu_1 \mu_2}{T^2}. \tag{35}$$

In the opposite limit the drag conductivity is independent of the properties of the second layer, since the integrals in Eq. (18b) are dominated by the region where both frequency and momentum are of order T. The single-layer conductivity in the second layer however is determined by μ_2 [see Eq. (32)] and thus

$$\rho_D(\mu_1 \ll T \ll \mu_2) \approx \alpha^2 \frac{\pi^2 \mathcal{N}_2}{8 \ln 2} \frac{\hbar}{e^2} \frac{\mu_1}{\mu_2} = 5.8 \alpha^2 \frac{\hbar}{e^2} \frac{\mu_1}{\mu_2}. \tag{36}$$

B. One layer with high carrier density

Secondly, if the chemical potential in one of the layers is much larger than temperature (without loss of generality we may also assume that the chemical potential of the other layer is also smaller)

$$\mu_2 \gg T, \quad \mu_2 > \mu_1,$$

then arguing along the lines of the previous subsection we find that the drag conductivity is independent of the largest chemical potential

$$\sigma_D = \alpha^2 e^2 T^2 \tau^2 f_2(\mu_1/T).$$

Again, we characterize the dimensionless function $f_2(x)$ by the two limits. The situation when the second layer is near its Dirac point was already discussed in the previous subsection. Therefore, similar to Eq. (34)

$$f_2(x \ll 1) \approx \mathcal{N}_2 x.$$

The drag coefficient in this case is given by Eq. (36).

In the case where $\mu_2 > \mu_1 \gg T$ the calculation is similar to that presented in Sec. II B. However now the combination of the hyperbolic functions [coming from the approximation (29)] in the momentum integral similar to Eq. (30) comprises two step functions and the integration is cut off by the smaller chemical potential. Hence

$$f_2(x \gg 1) \approx \frac{32}{3} \ln \frac{\mu_1}{T},$$

the drag conductivity is independent of the larger chemical potential μ_2. The drag coefficient in the limit of large μ_2 (but smaller than μ_1) is a generalization of Eq. (33)

$$\rho_D(\mu_2 > \mu_1 \gg T) \approx \alpha^2 \frac{\hbar}{e^2} \frac{8\pi^2}{3} \frac{T^2}{\mu_1 \mu_2} \ln \frac{\mu_1}{T}. \qquad (37)$$

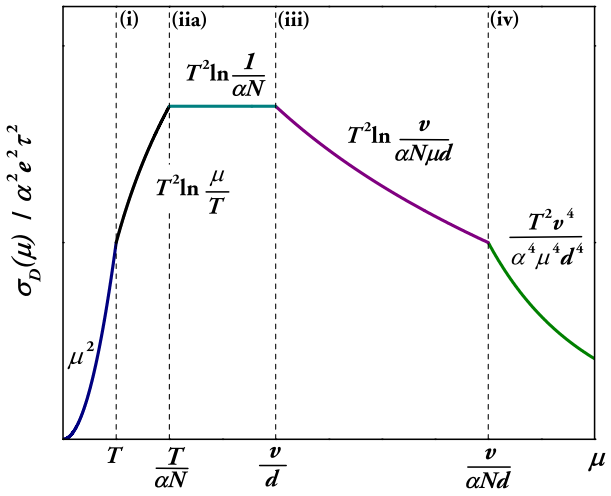

FIG. 3: [Color online] The sketch of the drag conductivity (in the units of $\alpha^2 e^2 \tau^2$) as a function of the chemical potential illustrating the results of Section IV A 1 in the case $T \ll N\alpha v/d$. The blue line corresponds to the quadratic dependence (25) in the vicinity of the Dirac point. The four regions at large chemical potentials correspond to the four regions discussed in Section IV A 1. If $T \gg N\alpha v/d$, then the region (iia) should be replaced by (ii), the logarithmic dependence $T^2 \ln(1/\alpha)$ should be replaced by $T^2 \ln[v/(Td)]$, and the limits v/d and $T/(N\alpha)$ should be exchanged.

IV. BEYOND THE LOWEST ORDER PERTURBATION THEORY

A. Finite inter-layer spacing and static screening

Let us now discuss what happens for non-zero inter-layer spacing d. For simplicity, we will consider the case of two identical layers. Generalization to the case of inequivalent layers is achieved along the lines of Sec. III.

1. *Vanishing interaction strength*

In the limit $\alpha \to 0$ the inter-layer spacing appears only in the exponential factor in the unscreened inter-layer interaction (8). Therefore, the momentum integration acquires a firm upper cut-off $q < v/d$, but the behavior at small momenta is unchanged.

As we have seen in Sec. II, the behavior of the drag coefficient in the vicinity of the Dirac point is determined by frequencies and momenta of the order of T (within our perturbation theory the single-layer conductivities in the two layers are independent of each other and d). Under the assumption (3) these momenta are small compared to v/d: taking into account the exponential in Eq. (8) yields a small correction to the numerical coefficient in Eqs. (27) and (35): $1.41 \to 1.41 + 4.06Td/v$.

In the opposite limit of low temperature we have found the behavior of the drag conductivity that is determined by large momenta. In the result (33) the upper limit of the logarithm is given by the chemical potential [due to the step-like behavior of the non-linear susceptibility (29)], while the lower limit is given by temperature as the typical value of frequency in Eq. (30).

Clearly, if finite d is taken into account then the logarithmic behavior in Eq. (33) may change: the upper limit of the logarithm will now depend on the relative value of the chemical potential and inverse inter-layer spacing.

At the same time the lower limit of the logarithm also depends on our approximations. Indeed, so far we have considered the effect of the unscreened inter-layer interaction. Consider now the role of the static screening. If both d and α are small then we may approximate the inter-layer interaction (9) by the expression

$$\mathcal{D}_{12}^R = -\frac{e^{-qd}}{\dfrac{q}{2\pi e^2} + 2\Pi^R}. \qquad (38)$$

At low temperatures the leading contribution to the static polarization operator is

$$\Pi^R(\omega = 0) = \frac{2k_F}{\pi v}. \qquad (39)$$

Thus the interaction propagator can be written as

$$\mathcal{D}_{12}^R = -\frac{2\pi\alpha v^2}{vq + 2N\alpha\mu}\, e^{-qd}.$$

Here $N = 4$ is due to spin and valley degeneracy. The unscreened interaction is a good approximation as long as the inverse screening length is small compared to typical momenta, i.e. as long as $N\alpha\mu \ll T$. In the opposite regime the lower limit of the logarithm in Eq. (31) will be determined by the screening length.

Combining the above arguments we conclude that increasing the chemical potential the following four regimes may be gradually achieved.

(i) $N\alpha\mu \ll T \ll \mu \ll v/d$. This regime was considered in Sec. II leading to Eqs. (31) and (33).

(ii) $N\alpha\mu \ll T \ll v/d \ll \mu$. If the chemical potential is increased beyond the inverse inter-layer spacing, then the momentum integration in Eq. (30) is cut off by v/d instead of μ. The logarithmic behavior of the drag conductivity Eq. (31) will be modified and σ_D no longer depends on the chemical potential

$$\sigma_D \sim \alpha^2 e^2 T^2 \tau^2 \ln \frac{v}{Td}. \tag{40}$$

(iia) $T \ll N\alpha\mu \ll \mu \ll v/d$. Depending on the actual values of T, d, and α it is possible that $N\alpha\mu$ exceeds temperature while the chemical potential is still smaller than the inverse inter-layer spacing $\mu \ll v/d$. Then instead of the previous regime we find

$$\sigma_D \sim \alpha^2 e^2 T^2 \tau^2 \ln \frac{1}{N\alpha}. \tag{41}$$

(iii) $T \ll N\alpha\mu \ll v/d \ll \mu$. Increasing the chemical potential further leads to the regime where the static screening can no longer be neglected. Now the lower integration limit in Eq. (30) is effectively given by the inverse screening length rather than the frequency. The upper limit is still determined by the inter-layer spacing. Therefore the drag conductivity again depends logarithmically on the chemical potential[24]

$$\sigma_D \sim \alpha^2 e^2 T^2 \tau^2 \ln \frac{v}{N\alpha\mu d}, \tag{42}$$

but now this is a *decreasing* function, indicating the existence of the absolute maximum of the drag conductivity as a function of the chemical potential.

(iv) $T \ll v/d \ll N\alpha\mu \ll \mu$. Finally, if the chemical potential is so large that the screening length becomes smaller than the inter-layer spacing the momentum integral in Eq. (30) is no longer logarithmic. In this regime we recover the standard Fermi-liquid result[3]. Note, that in this regime the step-like combination of the hyperbolic function in the non-linear susceptibility (29) is completely ineffective and may be replaced by unity. Given that in this regime the integration is dominated by momenta large compared to temperature the non-linear susceptibility may be further linearized in frequency. The resulting expression

$$\sigma_D = \frac{\zeta(3)}{4} \frac{e^2\tau^2T^2}{(k_F d)^2(\varkappa d)^2}, \quad \varkappa = 4\alpha k_F, \tag{43}$$

differs from that of Ref. 3 only by the factor reflecting valley degeneracy in graphene. Such expression for the drag conductivity was previously obtained in Ref. 20. The results of this subsection are illustrated in Fig 3.

2. *Intermediate interaction strength and $\mu \gg T$*

The above results rely on the smallness of the interaction strength α. However, if $N\alpha > 1$, then (i) the approximation (38) might not be justified and we would need to use the full expression (9) for the interaction propagator; (ii) the four regimes specified in the previous subsection may not exist, since it might happen that $T/(N\alpha) \ll T < v/(N\alpha d) \ll v/d$. In this case there are only two distinctive regimes (for $\mu \gg T$): (a) $\mu \ll v/d$, and (b) $\mu \gg v/d$. The latter regime is usually identified with the Fermi-liquid result[3,9,20,24,25], i.e. Eq. (43).

In this subsection we derive the approximate expression for the drag conductivity for large values of the chemical potential $\mu \gg T$, which accounts for the possibility of $N\alpha > 1$ (possible for small $\alpha \ll 1$, but large $N \gg 1$; here we still consider identical layers). In this regime the single-layer conductivity (32) is large (since $\mu\tau \gg T\tau \gg 1$) and therefore we can still limit our consideration to the diagram in Fig. 1. Moreover, for $\mu \gg T$ we can somewhat relax the condition (5) on the interaction strength and require the electron-electron scattering time to be larger than the impurity scattering time

$$\tau_{ee} \gg \tau \quad \Rightarrow \quad \tau^{-1} \gg \alpha^2 \frac{T^2}{\mu} \quad \Rightarrow \quad \alpha^2 T\tau \ll \frac{\mu}{T}.$$

Now we can follow the usual steps leading to the Fermi-liquid result (43). We consider only the static screening by approximating the polarization operator by Eq. (39) (see Appendix C for details). We further assume[23] that the dominant contribution to the drag conductivity comes from the region $vq > \omega$. Finally, we assume that in that region the result of the momentum integral is determined by the upper integration limit and is therefore independent of ω. This allows us to evaluate the frequency integral and represent the drag conductivity in terms of the single integral over momenta. Under these assumptions we find similarly to Eqs. (30)

$$\sigma_D = \alpha^2 e^2 T^2 \tau^2 f_0\left(\frac{\mu}{T}; \alpha; \frac{Td}{v}\right), \tag{44a}$$

$$f_0(x;\alpha;\lambda) \approx \frac{32}{3}\int_1^\infty \frac{dQQ^3 e^{-4\lambda Q}}{\left[(Q+\tilde\alpha(x))^2 - \tilde\alpha(x)^2 e^{-4\lambda Q}\right]^2} \times \frac{\sinh^2 x}{(\cosh Q + \cosh x)^2},$$

where

$$\tilde\alpha(x) = \frac{N}{2}\,\alpha x. \tag{44b}$$

Here we have approximated the function $g(x, |W| < Q)$ by Eq. (29), but neglected the frequency under the square root. In the limit $\mu \gg T$ the combination of the hyperbolic functions in $g(x, |W| < Q)$ has the form of the step function, which effectively cuts off the integration at $Q \sim x$. Thus we arrive at the approximate expression

$$f_0(x;\alpha;\lambda) \approx \frac{32}{3}\int_1^x \frac{dQQ^3 e^{-4\lambda Q}}{\left[(Q+\tilde\alpha(x))^2 - \tilde\alpha(x)^2 e^{-4\lambda Q}\right]^2}. \tag{44c}$$

The results of the previous subsection can now be recovered for $\alpha \ll 1$ by neglecting the terms proportional to $\tilde{\alpha}^2$ in the denominator. In contrast, the Fermi-liquid result (43) can be obtained by (i) assuming $\tilde{\alpha} \gg 1$ and keeping only the terms proportional to $\tilde{\alpha}^2$ in the denominator, (ii) assuming $x \gg 1/4\lambda$ and thus replacing the upper integration limit by infinity, and (iii) replacing the lower integration limit by zero. Moreover, for $\mu \gg v/d$ the integration limit can be extended such that the result becomes a function of one single parameter

$$f_0(x;\alpha;\lambda) \approx \tilde{f}_0(4\lambda\tilde{\alpha}), \tag{44d}$$

where

$$\tilde{f}_0(y) = \frac{32}{3}\int_0^\infty \frac{dZ Z^3 e^{-Z}}{\left[(Z+y)^2 - y^2 e^{-Z}\right]^2}. \tag{44e}$$

The function (44e) describes the crossover between the regimes (iii) and (iv) of the previous subsection (see Fig. 3). This can be seen by evaluating the integral in the two limits (here $\gamma_0 \approx 0.577216$ is the Euler's constant)

$$\tilde{f}_0(y \ll 1) \approx \frac{32}{3}\left(\ln\frac{1}{y} - \gamma_0 - \frac{11}{6}\right), \tag{45a}$$

$$\tilde{f}_0(y \gg 1) \approx \frac{64\zeta(3)}{y^4}. \tag{45b}$$

It turns out that by numerical reasons this crossover spans a large interval of values of the chemical potential such that the Fermi-liquid result (43) is practically unattainable in graphene-based drag measurements[9]. We illustrate this point in Figs. 4 - 5.

First of all we evaluate the whole expression (7). In order to do that we need to evaluate the full non-linear susceptibility (16). In addition we need to determine the polarization operator in graphene at finite temperature and chemical potential. In the ballistic regime we neglect the effect of disorder on the polarization operator. This is the only approximation in this calculation, see Appendix C for details. The role of the disorder is discussed in the following subsections. The corresponding data is shown in Figs. 4 - 5 by blue squares. Further results of the numerical evaluation of the drag conductivity (7) are shown in Appendix D.

Then we can simplify calculations by using the static approximation (39) for the polarization operator. The result of this calculation is shown in Figs. 4 - 5 by the red line. For weak interaction $\alpha = 0.01$ and relatively small inter-layer spacing (such that $Td/v = 0.1$) the results of the static screening approximation are indistinguishable from the "full" calculation as can be seen in Fig. 4. At the same time, for "intermediate" values[9,25] $\alpha = 0.3$, $Td/v = 0.2$, the static screening approximation "works" well for small and large chemical potentials, while somewhat overestimating the overall peak height.

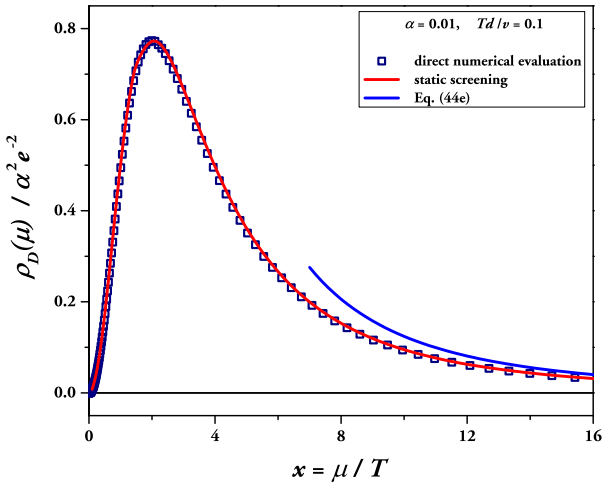

FIG. 4: [Color online] Results of the numerical evaluation of the drag coefficient for $\alpha = 0.01$ and $Td/v = 0.1$. The squares represent the calculation of Eq. (7) with the only approximation that the polarization operator in the screened inter-layer interaction (9) was evaluated in the absence of disorder. The red line corresponds to the same calculation, but replacing the polarization operator by Eq. (39), i.e. taking into account only static screening. The blue line corresponds to the approximate expression (44e),valid for $\mu \gg v/d$.

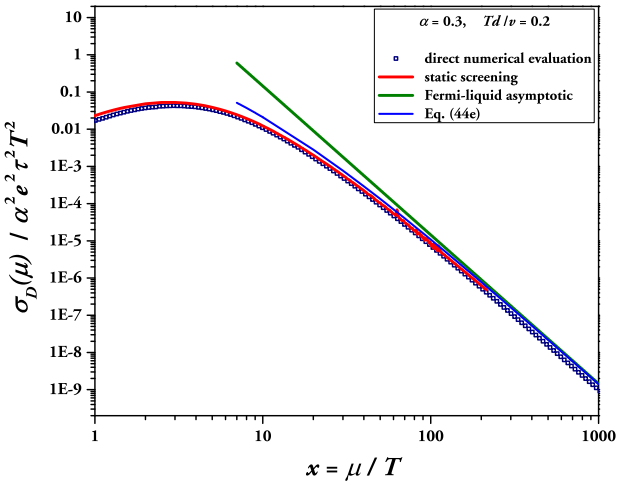

FIG. 5: [Color online] Results of the numerical evaluation of the drag conductivity for $\alpha = 0.3$ and $Td/v = 0.2$ shown in the log-log scale. The straight green line represents the Fermi-liquid result (43). The solid blue line corresponds to the approximate expression (44e),valid for $\mu \gg v/d$.

Finally, we can evaluate the approximate expression (44e). This expression was derived assuming $\mu \gg v/d$. For the parameter values used in Figs. 4 - 5 the expression (44e) fits the exact calculation for $\mu/T > 10$. However, the Fermi-liquid asymptotic (represented by the straight green line in Fig. 5) is not reached until $\mu/T > 200$. Clearly this is very far from the param-

eter regime relevant to the experimental observation of the Coulomb drag in graphene[9,25]. It is therefore not surprising that the Fermi-liquid-like approximations overestimate the observed values of the drag[9]. The data in Fig. 5 show that the asymptotic results, such as Eq. (43) may sometimes be achieved only at the extreme values of parameters. In order to describe the effect in the intermediate (or realistic) parameter regime, one needs to evaluate Eq. (7) with only minimal approximations.

B. Energy-dependent scattering time

The drag coefficient (21) and the asymptotic results of Sec. II and Sec. III, as well as the numerical data of Sec. IV A, were obtained assuming a constant impurity scattering time τ. In graphene, the scattering time strongly depends on the type of the impurities and usually depends on energy[26–30]. In the context of the Coulomb drag in graphene a similar issue (namely, the momentum-dependent scattering time) was investigated in Ref. 25 in the framework of the kinetic equation.

1. Non-linear susceptibility

Consider now the effect of the energy (or momentum) dependence of the scattering time. Within our assumption (5) we can still consider the ballistic Green's functions (A10), only now instead of being the overall factor, the scattering time is a part of the integrand in the non-linear susceptibility (12). Due to the δ-function form of the Green's functions we can focus on the energy-dependent τ regardless of the microscopic impurity model.

Repeating the steps leading to Eq. (16) with the energy-dependent $\tau(\epsilon)$ we find that the functions (16b) and (16b) become (see Appendices A and B for details)

$$g(x)=\begin{cases}\displaystyle\int_0^1 dz\frac{\sqrt{1-z^2}}{2\sqrt{\frac{W^2}{Q^2}-1}}\,I(z)K(z),\ |W|>Q,\\[2ex] \displaystyle\int_1^\infty dz\frac{\sqrt{z^2-1}}{2\sqrt{1-\frac{W^2}{Q^2}}}\,I(z)K(z),\ |W|<Q,\end{cases}\tag{46a}$$

where

$$K(z)=\frac{zW-Q}{zQ-W}\frac{\tau(T[zQ-W])}{\tau(T)}-\frac{zW+Q}{zQ+W}\frac{\tau(-T[zQ+W])}{\tau(T)},\tag{46b}$$

so that the explicit factor of the scattering time in Eq. (16a) should be understood as $\tau(T)$. This choice of the prefactor is not essential and is dictated by the discussion of the case $\mu\ll T$ below.

In the simple case $\tau(\epsilon)=const$, the function $K(z)$ simplifies to

$$K(z)=-2z\frac{1-W^2/Q^2}{z^2-W^2/Q^2},\tag{47}$$

and we recover Eqs. (16b) and (16b).

2. Vicinity of the Dirac point

Taking into account energy dependence of the scattering time $\tau(\epsilon)$ modifies the non-linear susceptibility and thus changes the Coulomb drag. In the limit $\mu\ll T$ the region $Q\sim W$ becomes important. As can be seen from Eqs. (16b) and (16b), if $\tau(\epsilon)=const$, then precisely at $Q=|W|$ the non-linear susceptibility vanishes. Otherwise, Eqs. (46) may contain a divergence.

Consider for example Coulomb scatterers. Then[26,27]

$$\tau(\epsilon)=\tau_0^2|\epsilon|.\tag{48}$$

In this case the function (47) depends on the relation between $|W|$ and Q

$$K(z)\to -2\begin{cases}Q, & Q>W,\\ z|W|, & Q<W,\end{cases}\tag{49}$$

and as a result the integral (18b) contains a logarithmic divergence at $Q=|W|$ since now

$$g(x_1)g(x_2)\propto|W^2-Q^2|^{-1}.\tag{50}$$

Same result holds for the case of strong short-ranged impurities that also yield the linear dependence $\tau\sim|\epsilon|$ (up to logarithmic renormalization which is inessential in the present context)[28].

Similarly, in the case of weak short-ranged disorder[29]

$$\tau^{-1}(\epsilon)=\gamma|\epsilon|,\tag{51}$$

the function (46b) does not vanish[21] for $Q=|W|$:

$$K(z)\to -2\begin{cases}Q\dfrac{z^2Q^2+W^2-2z^2W^2}{(z^2Q^2-W^2)^2}, & Q>|W|,\\[2ex] z|W|\dfrac{z^2Q^2+W^2-2Q^2}{(z^2Q^2-W^2)^2}, & Q<|W|.\end{cases}$$

Therefore the non-linear susceptibility contains the same logarithmic divergence (50).

Finally, even in the case of logarithmic renormalization of the scattering time[28,30] the function (47) does not vanish for $Q=|W|$ leading to Eq. (50). We conclude, that Eq. (50) is the generic behavior, while the vanishing (for $Q=|W|$) non-linear susceptibility (16) is the artifact of the approximation $\tau(\epsilon)=const$.

The divergence indicates that in the region $W\sim Q$ the δ-function approximation for the Green's functions

(A10) is invalid. Going beyond this approximation is qualitatively equivalent to regularizing the divergence by the scattering time $\tau(T)$. Thus the drag coefficient in the vicinity of the Dirac point acquires an additional logarithmic factor

$$\rho_D(\mu_1,\mu_2 \ll T) \sim \alpha^2 \frac{\hbar}{e^2}\frac{\mu_1\mu_2}{T^2}\ln T\tau(T). \qquad (52)$$

3. Low temperature limit

In the low temperature limit the non-linear susceptibility is determined by electrons near the Fermi surface and one can set ϵ in the triangular vertex (13) to be equal to the chemical potential. Then it appears that in all subsequent expressions one has to replace $\tau(\epsilon)$ by $\tau(\mu)$

$$\mu \gg T \quad \Rightarrow \quad \tau(\epsilon) \approx \tau(\mu). \qquad (53)$$

Let us understand this statement in more detail. Consider for example Coulomb scatterers. In the limit $\mu \gg T$ the non-linear susceptibility is dominated by $Q \gg W$. In this case we can evaluate the integral in Eq. (46a) using the function $K(z)$ from Eq. (49) and approximating $I(z)$ by Eq. (28). As a result we find

$$g(Q \gg W) = \frac{4W\sinh x}{\cosh Q + \cosh x} + \frac{4W}{Q}\ln\frac{e^{2x}+e^{x+Q}}{1+e^{x+Q}}$$
$$\simeq 4W\left[1+\frac{x}{Q}\right]\theta(x-Q). \qquad (54)$$

The momentum integral is still logarithmic. Therefore we can approximate $g(Q \gg W)$ by

$$g(Q \gg W) \approx \frac{4W}{Q}x,$$

which indeed recovers the statement (53) [notice that $\tau(T)x = \tau(\mu)$].

This argument is not restricted to Coulomb scatterers since in the limit $x \gg Q$ the function $I(z)$ in Eq. (28) is essentially a δ-function: $I(z) \approx -4W\delta(x - zQ)$. Therefore the function $K(z)$ in the integrand in Eq. (46) becomes $K(z) \to -2\tau(\mu)/[z\tau(T)]$ for an arbitrary $\tau(\epsilon)$.

In addition, the function g contains the divergence (50) at $Q \sim W$ which is always present for $\tau(\epsilon) \neq const$. Similarly to Eq. (52) this results in an additional logarithmic contribution (50), which is typically subleading. For example, the Fermi-liquid result (43) acquires an additional factor $1 + (Td/v)\ln T\tau(T)$. Thus we conclude that for $\mu \gg T$ taking into account the energy dependence of the impurity scattering time does not affect our results.

Finally, the divergence (50) appears only if both chemical potentials are small. Indeed, if $\mu_1 \ll T \ll \mu_2$, then while the non-linear susceptibility in the first layer is given by Eq. (46), in the second layer the scattering time may be replaced by its value at the chemical potential and thus Eq. (16) applies. Now the divergent denominator $|W^2 - Q^2|^{-1/2}$ of the former susceptibility is canceled by precisely the same factor in the numerator in the latter. Hence, the product $g(x_1)g(x_2)$ is finite at $|W| = Q$.

C. Plasmon contribution

The above results were obtained while neglecting the plasmon pole of the interaction propagator. Let's now estimate the plasmon contribution keeping α small. Consider for simplicity identical layers. In the limit $d \to 0$, the plasmon pole in the propagator of the inter-layer interaction is very similar to that of the single layer. Indeed, introducing dimensionless functions

$$\mathcal{D}_{12}^R = -\frac{2\pi e^2}{q}D, \quad \Pi^R = \frac{2q}{\pi^2 v}P, \qquad (55)$$

the inter-layer propagator (9) can be expressed as

$$D^{-1} = (1+\beta P)^2 e^{qd} - \beta^2 P^2 e^{-qd}, \quad \beta = \frac{4\alpha}{\pi}.$$

In the limit $d \to 0$ the pole corresponds to the solution of the equation

$$1 + 2\beta P = 0,$$

which differs from its single-layer counterpart by the factor of 2 only.

Now the drag conductivity (7) is determined by the product of the square of the interaction propagator and two non-linear susceptibilities. Using the dimensionless notations (55) and (16) we can write the integrand in Eq. (7) in the form

$$\Gamma_1^\alpha \Gamma_2^\beta |\mathcal{D}_{12}^R|^2 \propto e^2\tau^2\alpha^2 \frac{q^\alpha q^\beta}{q^2}\, g^2 |D|^2. \qquad (56)$$

Calculations of Sec. I C are essentially equivalent to arguments based on the Fermi Golden Rule yielding the perturbative result $\rho_D \sim \alpha^2$. Now we show that taking into account the plasmon contribution results in additional smallness, justifying the perturbative calculation of Sec. I C.

Plasmon modes in a single graphene sheet in the vicinity of the Dirac point were studied in Ref. 14. The plasmon pole appears in the region

$$W > Q.$$

Adjusting for the above factor of 2, the plasmon dispersion and decay rate are given by

$$W_p = \sqrt{\frac{Q}{Q+2\tilde\alpha}}\,(Q+\tilde\alpha), \quad \tilde\alpha = 8\alpha\ln 2, \qquad (57)$$

$$\Gamma_p = \frac{\pi\tilde\alpha^2}{16\ln 2}\left(\frac{Q}{Q+2\tilde\alpha}\right)^{3/2}(Q+\tilde\alpha). \qquad (58)$$

The plasmon contribution to the drag conductivity may be described by the following form of the inter-layer interaction propagator

$$|D|^2 \sim \frac{(W^2-Q^2)^3}{\tilde{\alpha}^2 Q^2}\frac{1}{(W-W_p)^2+\Gamma_p^2}.$$

At the same time, as argued in Ref. 14, the typical momenta dominating the relaxation rates are not too small

$$Q \gtrsim \tilde{\alpha}. \tag{59}$$

Then the decay rate is small $\Gamma_p \sim \tilde{\alpha}^3$ and the interaction propagator has the form of a sharp peak. Estimating the typical frequency at the peak by the plasmon dispersion we note that

$$W_p^2 - Q^2 = \frac{\tilde{\alpha}^2 Q}{Q+2\tilde{\alpha}} \sim \tilde{\alpha}^2, \tag{60}$$

and therefore the inter-layer interaction takes the form (omitting inessential numerical factors)

$$|D|^2 \sim \frac{\tilde{\alpha}^2}{(W-W_p)^2+\tilde{\alpha}^6}.$$

Consider now the non-linear susceptibility g. Typical momenta (59) are small enough, which allows us to approximate the non-linear susceptibility (16b) by its asymptotic value in the small $Q \to 0$ limit

$$g_1(Q\to 0) \approx \frac{\pi Q^2}{4W}. \tag{61}$$

As a result, for $Q \sim \tilde{\alpha}$,

$$g^2|D|^2 \propto \frac{\tilde{\alpha}^6}{(W-W_p)^2+\tilde{\alpha}^6} \to \tilde{\alpha}^3\delta(W-W_p).$$

For larger momenta $Q \sim 1$ the result is similar. The interaction propagator is now given by

$$|D|^2 \sim \frac{\tilde{\alpha}^4}{(W-W_p)^2+\tilde{\alpha}^4}.$$

At the same time the non-linear susceptibility (16) contains a factor $\sqrt{W^2-Q^2}$. Using Eq. (60), we find

$$g^2|D|^2 \propto \frac{\tilde{\alpha}^6}{(W-W_p)^2+\tilde{\alpha}^4} \to \tilde{\alpha}^4\delta(W-W_p).$$

If however, the temperature dependence of the scattering time is taken into account, then instead of vanishing at $|W|=Q$ the non-linear susceptibility contains the divergence (50) and thus a more careful analysis is necessary. Now we need to find the plasmon dispersion and decay rate at $T \neq 0$ in the presence of disorder. This complicated problem lies beyond the scope of the present paper. Here we estimate the plasmon contribution to σ_D in the most relevant region $Q \sim |W| \sim T$. It turns out that under our assumption (5) this contribution is small compared to the leading approximation (18).

In order to find the plasmon dispersion we need to calculate the polarization operator at $T \neq 0$ in the presence of disorder. This can be done with the help of the kinetic equation derived in Ref. 31. In comparison to the usual τ-approximation this equation contains an additional term describing the suppression of backscattering in graphene. It turns out that in the region $Q \sim |W| \sim T$ the polarization operator may be approximated by

$$\Pi^R = \frac{\partial n}{\partial \mu}\left[1 - \frac{i\omega}{\sqrt{\left(i\omega+\frac{1}{\tau}\right)^2 + v^2q^2}}\right], \tag{62}$$

where the thermodynamic density of states is given by

$$\frac{\partial n}{\partial \mu} = \frac{4T}{\pi v^2}\ln\left[2\cosh\frac{\mu}{2T}\right]. \tag{63}$$

The absence of the extra term $1/\tau$ in the denominator (c.f. Ref. 32) is precisely due to the suppression of backscattering: for arbitrary q and ω there is indeed a rather involved expression generalizing this term to the case of graphene, but for $Q \sim |W| \sim T$ this contribution is small and may be neglected.

Solving for the plasmon dispersion with the help of Eq. (62) we find

$$W_p \approx Q, \quad \Gamma_p = \tau^{-1}.$$

Thus the plasmon dispersion is changed little from Eq. (57), where for $Q \gg \tilde{\alpha}$ we also have $W_p \approx Q$. However the decay rate is now completely determined by disorder. Now the interaction propagator takes the form

$$|D|^2 \sim \frac{\tilde{\alpha}^4 T\tau}{Q^2}\frac{1/T\tau}{(W-W_p)^2+1/T^2\tau^2}.$$

Multiplying this expression by the diverging g^2, we notice that corrections to the linear plasmon dispersion are still determined by the interaction as in Eq. (60). Therefore, we find that the resulting contribution contains the small factor $\alpha^2 T\tau$ and is negligible under our assumption (5).

In order to estimate the drag conductivity we now need to integrate the product $g^2|D|^2$ over frequency and momentum, see Eqs. (7) and (56). This product contains a small factor of at least $\tilde{\alpha}^3$, or, if energy dependence of the scattering time is taken into account, a small parameter $\alpha^2 T\tau$. Therefore the plasmons contribute in the subleading order in the perturbative expansion in α.

The conclusions of this Section are confirmed by comparing the results of numerical evaluation of ρ_D using either the full dynamically screened interaction (9) or only the static screening, see Eq. (39). The results are illustrated in Figs. 4-5: the difference between the two results is only noticable for larger values of α. Thus taking into account plasmons does not lead to any new qualitative features of the theory.

D. Spectrum renormalization

If Coulomb interaction is taken into account, then the Dirac spectrum in graphene acquires logarithmic corrections[33]. This can be understood in terms of the renormalization of the interaction parameter α[34,35] and disorder strength[36]. The renormalization group flow terminates at $\max(\mu, T)$ and at lower energy scales we can treat the parameters α and v as scale-independent and equal to their renormalized values. The disorder scattering time retains its explicit energy dependence which follows from the microscopic impurity model.

In our calculation of the drag conductivity all frequency integrals are effectively cut off by temperature, while the momentum integrals are cut off by either T or μ, whichever is larger. In all of these cases we can treat the spectrum as linear with the renormalized velocity. Then our result (52) is still applicable, with the velocity and interaction parameter α taking the renormalized values $v[\max(\mu, T)]$ and $\alpha[\max(\mu, T)]$.

E. Experimental relevance

1. Carrier density

Experimental results[9] are expressed as a function of carrier density rather than the chemical potential as we have discussed in this paper. The relation between the carrier density n and the chemical potential μ can be obtained by integrating the density of states $\rho(\epsilon)$:

$$n = \int_{-\infty}^{\infty} d\epsilon \rho(\epsilon) \left[n_F(\epsilon; \mu) - n_F(\epsilon; 0) \right], \tag{64}$$

where $n_F(\epsilon; \mu)$ is the Fermi distribution function.

In graphene $\rho(\epsilon) = 2|\epsilon|/(\pi v^2)$ and the integral

$$n = \int_{-\infty}^{\infty} \frac{d\epsilon |\epsilon|}{\pi v^2} \left[\tanh \frac{\epsilon}{2T} - \tanh \frac{\epsilon - \mu}{2T} \right] \tag{65}$$

can be easily evaluated in the limiting cases [cf. Eq. (63)]

$$n = \frac{1}{\pi v^2} \begin{cases} \mu^2, & \mu \gg T, \\ (4 \ln 2) \mu T, & \mu \ll T, \end{cases} \tag{66}$$

which of course recovers the $T = 0$ expression for $\mu \gg T$.

If impurity scattering is taken into account then the density of states in the vicinity of the Dirac point saturates to a value determined by disorder[28]

$$n(\mu, T < \tau^{-1}) = \frac{\mu}{v^2 \tau}. \tag{67}$$

However for $T\tau \gg 1$ this effect is not important.

In experiment the carrier density may be obtained from measurements of the Hall coefficient in a non-quantizing magnetic field H. In graphene this is more complicated than in usual metals since the Hall coefficient vanishes at the Dirac point[37] due to electron-hole symmetry. While at low temperatures the behavior of the Hall coefficient is rather complicated[38], at high temperatures we can use the conventional Boltzmann kinetic equation with the energy-dependent cyclotron frequency[38] $\omega_c(\epsilon) = eHv^2/(c\epsilon)$. Then we find

$$\sigma_{xx} = -e^2 v^2 \int d\epsilon \frac{\partial n_F(\epsilon)}{\partial \epsilon} \frac{\rho(\epsilon) \tau_{tr}(\epsilon)}{1 + \omega_c^2(\epsilon) \tau_{tr}^2(\epsilon)}, \tag{68a}$$

$$\sigma_{xy} = -e^2 v^2 \int d\epsilon \frac{\partial n_F(\epsilon)}{\partial \epsilon} \frac{\rho(\epsilon) \omega_c(\epsilon) \tau_{tr}^2(\epsilon)}{1 + \omega_c^2(\epsilon) \tau_{tr}^2(\epsilon)}, \tag{68b}$$

Using Eqs. (68) at low temperatures $\mu \gg T$ and for weak magnetic fields H we of course recover the classic result

$$R_H = -\frac{\sigma_{xy}}{(\sigma_{xx}^2 + \sigma_{xy}^2) H} = -\frac{1}{nec},$$

with the electron density given by Eq. (66).

Exactly at the Dirac point the Hall conductivity vanishes, $\sigma_{xy}(\mu = 0) = 0$, as can be seen directly from Eq. (68b): all functions in the integrand, except for $\omega_c(\epsilon)$ are even in ϵ. For finite $\mu \ll T$ the Hall coefficient is linear in the chemical potential and thus linear in carrier density, as can be seen from Eq. (66).

$$R_H \propto \frac{\mu v^2}{ecT^3} = \frac{n}{n_*^2 ec}, \quad n_* \propto \frac{T^2}{v^2}.$$

The numerical coefficient in the above expression depends in the precise nature of impurities (see Sec. IV B).

2. Single-gate setup

At the time of writing, there is only one published report of a Coulomb drag measurement in graphene-based double-layer system[9]. In this experiment there is only one gate controlling the carrier density in both layers. The carrier densities can then be found by solving two electro-static equations[9,25]

$$eV_{BG} = \mu_B + e^2 (n_B + n_T)/C_1, \tag{69a}$$

$$\mu_B = \mu_T + e^2 n_T / C_2, \tag{69b}$$

where V_{BG} is the voltage applied to the bottom gate, μ_B and μ_T are the chemical potentials of the bottom and top layer respectively, C_1 is the capacitance of the oxide layer between the gate and the bottom layer, and C_2 is the capacitance of the inter-layer spacing.

Eqs. (69) were used in Ref. 25 to deduce that the gate voltage V_{BG} is proportional to the carrier density. Let us estimate the density n_B^* for which electrical and chemical potentials of the bottom layer become comparable:

$$n_B^*/C_1 = v\sqrt{\pi n_B^*} \;\; \Rightarrow \;\; n_B^* = \pi v^2 C_1 \sim 10^8 cm^{-2}. \tag{70}$$

Here the numerical value is estimated using the parameters of the experimental device[9,25]. Thus the linear relation $V_{BG} \propto n_B$ is valid for $n_B \gg n_B^*$, which is satisfied for all densities considered in Ref. 25.

In the vicinity of the Dirac point and in the presence of disorder [see Eq. (67)] all terms in Eqs. (69) are linear in carrier density. As a result, both n_B and n_T are proportional to the gate voltage V_{BG} and in particular

$$V_{BG} \propto \mu_B.$$

According to Ref. 9 the carrier density in the top layer depends on V_{BG} only weakly and remains finite when the bottom layer is tuned to the vicinity of the Dirac point, such that $\mu_B < \mu_T$. In such conditions the drag coefficient is described by Eq. (36). Since in this regime the gate voltage seems to affect mostly the bottom gate of the device used in Ref. 9, we conclude that when the bottom layer is tuned towards the Dirac point, the drag should vanish linearly with the gate voltage. This conclusion is consistent with the experimental results of Ref. 9.

At the large carrier densities the drag should vanish as some power of the gate voltage as shown in Fig. 2. Since in the experiment the Fermi wavelength and the inter-layer spacing are of the same order of magnitude, the decay of the drag coefficient at large μ is described by Eq. (37). Neglecting the weak dependence of n_T on the gate voltage reported in Ref. 9, we conclude that

$$\rho_D \sim n_B^{-1},$$

which qualitatively agrees with the experimental results.

Given that the drag vanishes both at small and large μ (or gate voltages, or carrier densities), there must be a maximum at some intermediate value of μ, which is determined by temperature and sample geometry. Thus the results of the perturbation theory, as shown in Fig. 2, qualitatively describe all features of the drag observed in the experiment. Moreover, for relatively small values of the interaction parameter[25] $\alpha \approx 0.2$ our theory yields a reasonable quantitative description of the effect. The extension of our work for even stronger interaction and/or vanishing disorder will be published separately[15].

3. *Symmetric setup*

Another possibility[39] is to align the Dirac points in the two layers using a combination of gates and then apply a voltage $\mathcal{V}$ between the two layers, inducing same number of electrons in one layer and holes in another (such that $n_1 = n_2 = n$ and $\mu_1 = -\mu_2 = \mu$). In this case the results of Sec. I C and IV A apply.

The inter-layer voltage $\mathcal{V}$ is related to the carrier density by $\mathcal{V} = e^2 n/C + 2\mu$. The capacitance C is the only independently measurable coefficient in this relation and may be found by measuring the Hall coefficient at a large chemical potential. Then the $\mathcal{V}$-dependence of any quantity can be directly translated into the density dependence (using Eq. (65) to convert μ to n).

V. CONCLUSIONS

We have presented the perturbative theory of the Coulomb drag in ballistic graphene-based double-layer structures. Our theory is applicable to the wide range of temperatures and carrier densities, but is subject to the condition (5). In addition we have limited our discussion to the experimental[9] condition (3), the former is necessary to justify the theoretical approach that we've adopted in this paper. As shown in Sec. IV, Eq. (5) allows us to simplify our calculations by disregarding the effects of plasmon modes, Dirac spectrum renormalization, and energy dependent impurity scattering time. Eq. (5) also justifies our assumption that impurity scattering dominates the transport properties in the system.

The main results of this paper can be summarized as follows. Qualitatively, $\rho_D(\mu/T)$ has the same shape in all parameter regimes: in the vicinity of the Dirac point $\rho_D \propto \mu^2/T^2$, $\mu \sim T$ the drag reaches its maximum and then decays at $\mu \gg T$. This decay occurs over a wide region of μ where ρ_D cannot be described by a single power law. In particular, we have analyzed three regimes: (i) in the limit $\alpha \to 0$ and $d \to 0$ the drag coefficient is given by Eqs. (35), (36), and (37), see also Table I; (ii) for $\alpha \to 0$, but finite d the drag coefficient acquires logarithmic corrections, see Fig. 3; (iii) for intermediate interaction strength and $\mu \gg T$ we describe the crossover between the logarithmic and the Fermi-liquid behavior, see Eq. (44e). The latter occurs only at the largest values of μ, such that $\varkappa d \gg 1$. Thus our theory describes all qualitative features observed in Ref. 9.

Formally our results are applicable in the limit of weak interaction. The actual value of α in physical graphene is still the subject of a debate. Recent experiments[40,41] suggest that at experimentally relevant temperatures the effective (or renormalized) interaction parameter is rather small. In addition, if one takes into account dielectric properties of the substrate and/or the insulating layer between the two graphene sheets in the double-layer device[25], then the effective value of α will be even smaller.

For ultra-clean graphene, where transport is dominated by electron-electron interaction, our theory should be generalized for stronger interaction. In this case also the single-layer conductivity becomes non-trivial. In our opinion, the most adequate method for such calculations is the method of the kinetic equation[11,12,14]. Our work in this direction will be reported elsewhere[15].

Acknowledgments

We acknowledge helpful conversations with A.K. Geim, M.I Katsnelson, K.S. Novoselov, L. Ponomarenko, M. Schütt, and A. Shnirman. This research was supported by the Center for Functional Nanostructures of the Deutsche Forschungsgemeinschaft (DFG) and by SPP 1459 "Graphene" of the DFG. M.T. is grateful to KIT for hospitality.

Appendix A: Non-linear susceptibility in graphene

Here we derive the non-linear susceptibility (14) and consider a few limiting cases.

The general definition of the non-linear susceptibility is given by Eq. (11), which we repeat here for convenience:

$$\mathbf{I} = \int d\boldsymbol{r}_1 \int d\boldsymbol{r}_2 \mathbf{\Gamma}(\omega; \boldsymbol{r}_1, \boldsymbol{r}_2) V(\boldsymbol{r}_1) V(\boldsymbol{r}_2). \tag{A1}$$

Furthermore, Eqs. (12) and (13) express the non-linear susceptibility of a disordered conductor in terms of exact Green's functions of the system (for detailed derivation see Refs. 3,17):

$$\mathbf{\Gamma} = \int \frac{d\epsilon}{2\pi} \Bigg[\left(\tanh \frac{\epsilon - \mu}{2T} - \tanh \frac{\epsilon + \omega - \mu}{2T} \right) \boldsymbol{\gamma}_{12}(\epsilon; \omega) + \left(\tanh \frac{\epsilon - \mu}{2T} - \tanh \frac{\epsilon - \omega - \mu}{2T} \right) \boldsymbol{\gamma}_{21}(\epsilon; -\omega) \Bigg], \tag{A2}$$

$$\boldsymbol{\gamma}_{12}(\epsilon; \omega) = \Big[G^R_{12}(\epsilon + \omega) - G^A_{12}(\epsilon + \omega) \Big] G^R_{23}(\epsilon) \hat{\mathbf{J}}_3 G^A_{31}(\epsilon). \tag{A3}$$

In contrast to the usual Fermi Liquid calculation[3] we shift the chemical potential from the Green's functions into the distribution functions.

Averaging over disorder restores translational invariance. Moreover, in ballistic regime the Green's functions can be averaged independently. However, in graphene the eigenfunctions of the Dirac Hamiltonian are not plane waves. Focusing on a given valley and spin projection, we can write down the Dirac Hamiltonian as

$$\mathcal{H} = vk \begin{pmatrix} 0 & e^{i\varphi_{\boldsymbol{k}}} \\ e^{-i\varphi_{\boldsymbol{k}}} & 0 \end{pmatrix}, \ \cos\varphi_{\boldsymbol{k}} = \frac{k_x}{k}, \ \sin\varphi_{\boldsymbol{k}} = \frac{k_y}{k}. \tag{A4}$$

The electron field operator in the basis of eigenstates can be written as

$$\widehat{\Psi}(\boldsymbol{r}) = \frac{1}{\sqrt{2}} \sum_{\boldsymbol{k},\nu} e^{i\boldsymbol{k}\boldsymbol{r}} \begin{pmatrix} \nu e^{-i\varphi_{\boldsymbol{k}}} \\ 1 \end{pmatrix} \widehat{c}_{\boldsymbol{k},\nu}, \tag{A5}$$

where $\nu = \pm$ is the band index and the spinor [as well as the Hamiltonian (A4)] is written in the sublattice space. In the basis of the eigenstates the (disorder-averaged) Green's functions are diagonal:

$$G^R_\nu(\epsilon, \boldsymbol{k}) = \frac{1}{\epsilon - E_\nu(\boldsymbol{k}) + i/2\tau(\boldsymbol{k})}, \quad E_\nu(\boldsymbol{k}) = \nu v k. \tag{A6}$$

The impurity scattering time $\tau(\boldsymbol{k})$ may in general depend on momentum of the scattering states (see Appendix B).

Now we can write the triangular vertex $\boldsymbol{\gamma}$ in the form:

$$\boldsymbol{\gamma}(\epsilon; \omega, \boldsymbol{q}) = N \sum_{\nu\nu'} \int \frac{d^2k}{(2\pi)^2} \left| \lambda^{\nu,\nu'}_{\boldsymbol{k},\boldsymbol{k}+\boldsymbol{q}} \right|^2 \times \mathrm{Im} G^R_{\nu'}(\epsilon + \omega; \boldsymbol{k} + \boldsymbol{q}) G^R_\nu(\epsilon; \boldsymbol{k}) \widehat{\boldsymbol{j}}^{\,\mathrm{tr}}_\nu G^A_\nu(\epsilon; \boldsymbol{k}). \tag{A7}$$

The factor $N = 4$ reflects the spin and valley degeneracy, and

$$\left| \lambda^{\nu,\nu'}_{\boldsymbol{k},\boldsymbol{k}'} \right|^2 = \frac{1}{2} \left(1 + \nu\nu' \frac{\boldsymbol{k}\boldsymbol{k}'}{kk'} \right). \tag{A8}$$

The current operator[42] should also be written in the basis of the eigenstates where, unlike the original Bloch basis[22], the current operator depends on the direction of the quasi-particle momentum

$$\widehat{\boldsymbol{j}}^{\,\mathrm{tr}}_\nu = 2ev\nu \boldsymbol{n}_{\boldsymbol{k}}, \quad \boldsymbol{n}_{\boldsymbol{k}} = \boldsymbol{k}/k. \tag{A9}$$

The factor of 2 in Eq. (A9) appears due to the absence of backscattering in graphene: the transport time τ_{tr} is twice the scattering time[22].

Finally, in the ballistic regime $1/\tau \to 0$ and the Green's functions (A6) can be written in the form

$$G^R_\nu(\epsilon; \boldsymbol{k}) G^A_\nu(\epsilon; \boldsymbol{k}) \approx 2\pi\tau(\epsilon) \delta\Big(\epsilon - E_\nu(\boldsymbol{k}) \Big), \tag{A10a}$$

$$\mathrm{Im} G^R_\nu(\epsilon; \boldsymbol{k}) \approx -\pi \delta\Big(\epsilon - E_\nu(\boldsymbol{k}) \Big). \tag{A10b}$$

Here we have replaced the momentum dependence of the scattering time by the energy dependence given the δ-function approximation to the Green's functions. Note, that since Eq. (A7) does not contain any energy integration, this dependence plays no role in the triangular vertex $\boldsymbol{\gamma}$, which in ballistic regime takes the form

$$\boldsymbol{\gamma}(\epsilon; \omega, \boldsymbol{q}) = -Nev\tau(\epsilon) \sum_{\nu\nu'} \nu \int d^2k \, \boldsymbol{n}_{\boldsymbol{k}} \left| \lambda^{\nu,\nu'}_{\boldsymbol{k},\boldsymbol{k}+\boldsymbol{q}} \right|^2 \times \delta(\epsilon - \nu v k) \delta\left(\epsilon + \omega - \nu' v |\boldsymbol{k} + \boldsymbol{q}| \right). \tag{A11}$$

Using the δ-functions in Eq. (A11) we notice, that in Eq. (A11) the momenta satisfy

$$k^2 = \epsilon^2/v^2, \quad (\boldsymbol{k} + \boldsymbol{q})^2 = (\epsilon + \omega)^2/v^2, \tag{A12}$$

and therefore

$$\boldsymbol{k}\boldsymbol{q} = \frac{(\epsilon + \omega)^2 - \epsilon^2 - v^2 q^2}{2v^2} = \frac{\omega^2 + 2\epsilon\omega - v^2 q^2}{2v^2}. \tag{A13}$$

Now we can replace the momentum dependence of the vertices $\lambda^{\nu,\nu'}_{\boldsymbol{k},\boldsymbol{k}+\boldsymbol{q}}$ by the frequency dependence:

$$\left| \lambda^{\nu,\nu'}_{\boldsymbol{k},\boldsymbol{k}+\boldsymbol{q}} \right|^2 = 1 + \frac{\omega^2 - v^2 q^2}{4\epsilon(\epsilon + \omega)}. \tag{A14}$$

Then the triangular vertex (A11) becomes

$$\boldsymbol{\gamma}(\epsilon; \omega, \boldsymbol{q}) = -Nev\tau(\epsilon) \left[1 + \frac{\omega^2 - v^2 q^2}{4\epsilon(\epsilon + \omega)} \right] \boldsymbol{g}, \tag{A15}$$

$$\boldsymbol{g} = \sum_{\nu\nu'} \nu \int d^2k \, \boldsymbol{n}_{\boldsymbol{k}} \delta(\epsilon - \nu v k) \delta\left(\epsilon + \omega - \nu' v |\boldsymbol{k} + \boldsymbol{q}| \right). \tag{A16}$$

Clearly, the direction of the vector $\boldsymbol{g}$ coincides with the direction of $\boldsymbol{q}$:

$$\boldsymbol{g} = A\boldsymbol{q} \quad \Rightarrow \quad \boldsymbol{g} = \boldsymbol{q}\frac{(\boldsymbol{g}\boldsymbol{q})}{q^2},$$

$$\boldsymbol{g}\boldsymbol{q} = \sum_{\nu\nu'} \nu \int d^2k \frac{\boldsymbol{k}\boldsymbol{q}}{k} \delta(\epsilon - \nu v k)\delta\left(\epsilon + \omega - \nu' v|\boldsymbol{k}+\boldsymbol{q}|\right).$$

Here we can again use Eq. (A13) and therefore

$$\boldsymbol{g} = \boldsymbol{q}\frac{\omega^2 + 2\epsilon\omega - v^2q^2}{2v^2q^2} g_0, \tag{A17}$$

$$g_0 = \sum_{\nu\nu'} \nu \int \frac{d^2k}{k}\, \delta(\epsilon - \nu v k)\delta\left(\epsilon + \omega - \nu' v|\boldsymbol{k}+\boldsymbol{q}|\right). \tag{A18}$$

The remaining integration is straightforward and we find

$$g_0 = \frac{4|\epsilon+\omega|\theta_0(\epsilon,\omega,q)}{\sqrt{(v^2q^2-\omega^2)\left([2\epsilon+\omega]^2 - v^2q^2\right)}}, \tag{A19}$$

where ($\theta(x)$ is the Heaviside θ-function)

$$\theta_0(\epsilon,\omega,q) = \theta(vq - |2\epsilon+\omega|)\left[\theta(-\omega-vq) - \theta(\omega - vq)\right] + \theta(vq-|\omega|)\left[\theta(2\epsilon+\omega-vq) - \theta(-vq-2\epsilon-\omega)\right]. \tag{A20}$$

Now the triangular vertex gamma can be written using Eqs. (A15), (A17), (A19), and (A20) in the form (14)

$$\boldsymbol{\gamma}(\epsilon,\omega,q) = -\boldsymbol{q}Nev\tau(\epsilon)\frac{\omega^2+2\epsilon\omega - v^2q^2}{2\epsilon v^2q^2}\sqrt{\frac{[2\epsilon+\omega]^2 - v^2q^2}{v^2q^2-\omega^2}}\,\mathrm{sgn}(\epsilon+\omega)\theta_0(\epsilon,\omega,q). \tag{A21}$$

The function $\theta_0(\epsilon,\omega,q)$ is antisymmetric under the simultaneous change of sign of both frequencies

$$\theta_0(\epsilon,\omega,q) = -\theta_0(-\epsilon,-\omega,q).$$

Therefore the triangular vertex $\boldsymbol{\gamma}$ as a whole is symmetric under the simultaneous change of sign of all variables:

$$\boldsymbol{\gamma}(\epsilon,\omega,\boldsymbol{q}) = \boldsymbol{\gamma}(-\epsilon,-\omega,-\boldsymbol{q}). \tag{A22}$$

Using this property in Eq. (A2) we find the expression for the non-linear susceptibility in graphene:

$$\boldsymbol{\Gamma} = -\frac{Nev\boldsymbol{q}}{2\pi}\, g(\omega,q;\mu), \tag{A23a}$$

$$g(\omega,q;\mu) = \int d\epsilon \tau(\epsilon) I(\epsilon,\omega) F(\epsilon,\omega;q)\theta_0(\epsilon,\omega,q), \tag{A23b}$$

$$F(\epsilon,\omega;q) = \frac{\omega^2+2\epsilon\omega - v^2q^2}{2\epsilon v^2q^2}\sqrt{\frac{[2\epsilon+\omega]^2-v^2q^2}{v^2q^2-\omega^2}}\,\mathrm{sgn}(\epsilon+\omega), \tag{A23c}$$

$$I(\epsilon,\omega) = \tanh\frac{\epsilon-\mu}{2T} - \tanh\frac{\epsilon+\omega-\mu}{2T} - \tanh\frac{\epsilon+\mu}{2T} + \tanh\frac{\epsilon+\omega+\mu}{2T}. \tag{A23d}$$

The expression (16) then follows after a change of variables indicated in the text preceding Eq. (16) and explicitly resolving the integration limits given by Eq. (A20).

Comparing Eq. (A23) with the standard Fermi liquid result of Ref. 3, we should recall that within the Fermi liquid theory the Fermi energy is the largest energy scale in the problem. In order to compare Eq. (A22) to the corresponding results of Ref. 3, we consider the limit

$$\omega, vq \ll \epsilon \sim E_F.$$

In this limit the leading contribution to the functions in the integrand in Eq. (A23) is given by

$$F(\omega, vq \ll \epsilon) \approx \frac{\omega\epsilon}{v^2q^2}\frac{1}{\sqrt{v^2q^2-\omega^2}} - \frac{\sqrt{v^2q^2-\omega^2}}{2v^2q^2},$$

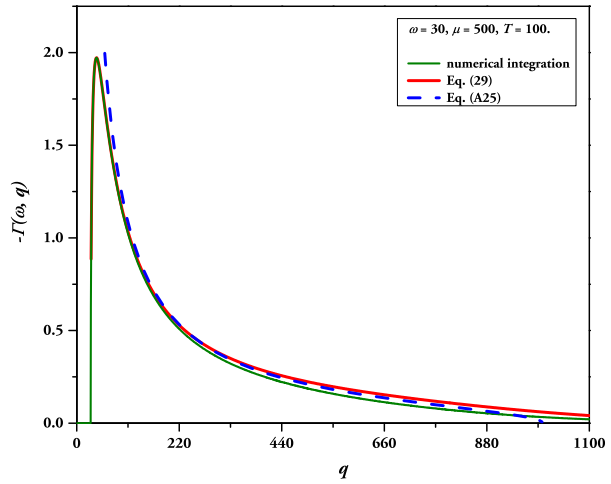

FIG. 6: [Color online] A numerical comparison of the approximations (29) and (A25). The former is shown by the red solid line, while the latter - by the blue dashed line. The solid green line is the numerical evaluation of Eq. (A23).

$$I_2(\omega \ll \epsilon) \approx \frac{\omega}{2T}\left[\frac{\theta(\epsilon)}{\cosh^2\frac{\epsilon+\mu}{2T}} - \frac{\theta(-\epsilon)}{\cosh^2\frac{\epsilon-\mu}{2T}}\right].$$

Thus all three terms F, I_2, and θ_0 in the integrand are odd functions of ϵ and as a result the leading contribution to non-linear susceptibility vanishes[18,19]. The subleading contribution (stemming from the second term in the function F) yields for $vq \gg \omega$

$$g(\omega, q) \approx -4\omega/vq, \tag{A24}$$

in agreement with Ref. 3. Same result is given also by Eq. (29) in the limit $\mu \gg T$ for $vq > \omega$.

The result (A24) was obtained assuming that typical values of momentum q are small compared to the Fermi momentum. This is justified for large inter-layer spacing $\varkappa d \gg 1$, which was assumed in Ref. 3. However, in graphene-based samples of Ref. 9 the inter-layer spacing is rather small and $\varkappa d \sim 1$. In this case we can no longer assume the momentum q to be small. Expanding the integrand in Eq. (A23) in the limit $\omega \ll vq, \epsilon \sim E_F$, we find

$$F(\omega \ll vq, \epsilon) \approx -\frac{1}{2vq}\sqrt{1-\frac{v^2q^2}{4\epsilon^2}},$$

while the expansion of I_2 remains the same as above. Now the frequency integration yields

$$g(\omega \ll q) \approx -4\frac{\omega}{vq}\sqrt{1-\frac{q^2}{4k_F^2}}. \tag{A25}$$

This expression approximates the non-linear susceptibility in the region $\omega \ll vq < 2E_F$. Comparing Eq. (A25) to Eq. (29) we note that both approximations work well in that intermediate region, see Fig. 6. At the same time, Eq. (29) accounts better for the behavior at $q \sim \omega$ and also allows for momenta larger than $2k_F$. Note, that the non-linear susceptibility (A23) is real, the fact that Eq. (A25) yields imaginary values for $q > 2k_F$ is the artifact of its approximate derivation.

Appendix B: Kinetic equation approach to drag in graphene

In this Appendix we derive the general expression for drag conductivity σ_D in the framework of the kinetic equation (this is justified by requiring large single-layer conductivity $\sigma_{1(2)} \gg e^2$, which is valid for $\mu \gg T$ or $\mu \gg \tau$). By solving the two coupled equations for the distribution functions of two graphene layers we will reproduce the result (7) with the nonlinear susceptibility $\mathbf{\Gamma}(\omega, \boldsymbol{q})$ given by Eqs. (12) and (14).

In Appendix A we have characterized the eigenstates (A5) of the massless Dirac Hamiltonian $H = v\boldsymbol{\sigma}\boldsymbol{k}$ [see also Eq. (A4)] by the value of momentum $\boldsymbol{k}$ and the discrete variable $\nu = \pm 1$ indexing conduction and valence bands. In this representation, the electron energy and velocity are $E_\nu(\boldsymbol{k}) = \nu v k$ and $\boldsymbol{v} = \nu v \boldsymbol{e_k}$ (where $\boldsymbol{e_k} = \boldsymbol{k}/k$ is the unit vector pointing in the direction of momentum).

Now for the purposes of deriving the kinetic equation, we find it more convenient to label the eigenstates by their energy ϵ and the unit vector $\boldsymbol{e_v} = \boldsymbol{v}/v$. The particle momentum is then $\boldsymbol{k} = \boldsymbol{e_v}E_\nu(\boldsymbol{k})/v$ and the eigenstates are normalized as follows

$$\int \frac{|\epsilon|\, d\epsilon\, d\boldsymbol{e_v}}{(2\pi v)^2}\, |\epsilon, \boldsymbol{e_v}\rangle\langle\epsilon, \boldsymbol{e_v}| = 1. \tag{B1}$$

In the lowest order of the perturbation theory we neglect electron-electron interaction within each layer and disregard the back action of the drag current in the passive layer onto the distribution function in the active layer. As a result the kinetic equation for the active layer is effectively decoupled and has the form

$$e\boldsymbol{E}\boldsymbol{v}\,\frac{\partial f_a}{\partial \epsilon} = \frac{\langle f_a\rangle - f_a}{\tau_a(\epsilon)}. \tag{B2}$$

Here $\boldsymbol{E}$ is the applied electric field and $\tau_a(\epsilon)$ is the transport time due to disorder scattering. Index a refers to the active layer. The distribution function depends on ϵ and $\boldsymbol{e_v}$; angular brackets denote averaging with respect to the velocity direction. Within linear response we substitute the equilibrium distribution function $f_a^{(0)}$ in the left-hand side of Eq. (B2) and find the following solution

$$f_a = f_a^{(0)} - \tau_a(\epsilon)\frac{\partial f_a^{(0)}}{\partial \epsilon}\, e\boldsymbol{E}\boldsymbol{v} = f_a^{(0)} + \tau_a(\epsilon) f_a^{(0)}\big(1 - f_a^{(0)}\big)\frac{e\boldsymbol{E}\boldsymbol{v}}{T}. \tag{B3}$$

This is equation is written for the case of "dirty" graphene $\tau_{dis}^{-1} \gg \tau_{ee}^{-1}$. The opposite limit of clean graphene will be discussed in Ref. 15.

Consider now the passive layer. We denote the corresponding distribution function f_b and include the collision term describing inter-layer scattering. The second kinetic equation has the form

$$0 = \frac{\langle f_b\rangle - f_b}{\tau_b} + \sum_{a,a',b'} w(a,b;\ a',b')\Big[f_a' f_b'(1-f_a)(1-f_b) - f_a f_b(1-f_a')(1-f_b')\Big]. \tag{B4}$$

Here $w(a,b;\ a',b')$ is the probability of scattering $(a',b') \mapsto (a,b)$, indices a, b, a', and b' label incoming and scattered states in both layers. Summation over these states is carried out according to their normalization (B1).

The drag current can now be expressed as

$$\boldsymbol{j}_D = e\sum_b \boldsymbol{v}_b f_b = e\sum_{a,a',b,b'} \tau_b \boldsymbol{v}_b\, w(a,b;\ a',b')\Big[f_a' f_b'(1-f_a)(1-f_b) - f_a f_b(1-f_a')(1-f_b')\Big]. \tag{B5}$$

Now we substitute equilibrium distributions in layer b, and the result (B3) for f_a and f_a'. Keeping only the terms linear in the external field $\boldsymbol{E}$ and using the momentum conservation law, we express the drag current as $j_D^\alpha = \sigma_D^{\alpha\beta}E^\beta$. Using the time-reversal invariance of the scattering probability, $w(a,b;\ a',b') = w(a',b';\ a,b)$, we represent the resulting drag conductivity in the symmetric form

$$\sigma_D^{\alpha\beta} = -\frac{e^2}{2T}\sum_{a,a',b,b'} (\tau_b'\boldsymbol{v}_b' - \tau_b\boldsymbol{v}_b)_\alpha(\tau_a'\boldsymbol{v}_a' - \tau_a\boldsymbol{v}_a)_\beta\, w(a,b;\ a',b')\ f_a' f_b'(1-f_a)(1-f_b). \tag{B6}$$

Here all distribution functions are taken at thermal equilibrium and the superscripts are suppressed for brevity. Each of the four scattering times entering the above equation is taken at the corresponding energy.

The transition probability $w(a,b;\ a',b')$ can be written with the help of the Fermi golden rule:

$$w(a,b;\ a',b') = \big|\langle a,b|U|a',b'\rangle\big|^2 (2\pi)^3\delta(\epsilon_a + \epsilon_b - \epsilon_a' - \epsilon_b')\,\delta(\boldsymbol{k}_a + \boldsymbol{k}_b - \boldsymbol{k}_a' - \boldsymbol{k}_b'), \tag{B7}$$

where the matrix element of the inter-layer interaction includes the Dirac factors (A8), re-written in terms of the velocities:

$$\big|\langle a,b|U|a',b'\rangle\big|^2 = \big|U\left(\boldsymbol{k}_a - \boldsymbol{k}_a'\right)\big|^2\ \frac{1+\boldsymbol{e}_{\boldsymbol{v}}^{(a)}\boldsymbol{e}_{\boldsymbol{v}}^{(a')}}{2}\ \frac{1+\boldsymbol{e}_{\boldsymbol{v}}^{(b)}\boldsymbol{e}_{\boldsymbol{v}}^{(b')}}{2}. \tag{B8}$$

With this matrix element, we can separate the quantities related to layers a and b in the expression for drag conductivity (B6). This allows us to represent it in the form of Eq. (7):

$$\sigma_D^{\alpha\beta} = \frac{e^2}{8T}\int \frac{d^2q\ d\omega\ |U(q)|^2}{(2\pi)^3\ \sinh^2\frac{\omega}{2T}}\Gamma_a^\alpha(\boldsymbol{q},\omega)\Gamma_b^\beta(-\boldsymbol{q},-\omega), \tag{B9}$$

$$\boldsymbol{\Gamma}_a(\boldsymbol{q},\omega) = (e^{\omega/T}-1)\sum_{a,a'} f_a'(1-f_a)(\tau_a'\boldsymbol{v}_a' - \tau_a\boldsymbol{v}_a)\frac{1+\boldsymbol{e}_{\boldsymbol{v}}^{(a)}\boldsymbol{e}_{\boldsymbol{v}}^{(a')}}{2}\ (2\pi)^3\delta(\epsilon_a - \epsilon_a' + \omega)\,\delta(\boldsymbol{k}_a - \boldsymbol{k}_a' + \boldsymbol{q}) \tag{B10}$$

and the same formula for $\boldsymbol{\Gamma}_b$. Note the symmetry relations $\boldsymbol{\Gamma}(-\boldsymbol{q},-\omega) = -\boldsymbol{\Gamma}(\boldsymbol{q},-\omega) = \boldsymbol{\Gamma}(\boldsymbol{q},\omega)$.

Let us now evaluate the expression (B10). Using the energy-velocity basis and resolving the energy delta function, we represent $\boldsymbol{\Gamma}$ as an integral over ϵ and over two velocity directions $\boldsymbol{e}_{\boldsymbol{v}}$ and $\boldsymbol{e}_{\boldsymbol{v}}'$. With equilibrium Fermi distribution functions, this yields

$$\boldsymbol{\Gamma}(\boldsymbol{q},\omega) = \frac{\boldsymbol{q}}{8\pi v q^2}\int d\epsilon\,|\epsilon(\epsilon+\omega)|\ \left[\tanh\frac{\epsilon+\omega-\mu}{2T} - \tanh\frac{\epsilon-\mu}{2T}\right] J(\epsilon,\epsilon+\omega,q), \tag{B11}$$

$$J(\epsilon,\epsilon',q) = \int d\boldsymbol{e}_{\boldsymbol{v}}\, d\boldsymbol{e}_{\boldsymbol{v}}'\,(\tau'\boldsymbol{q}\boldsymbol{e}_{\boldsymbol{v}}' - \tau\boldsymbol{q}\boldsymbol{e}_{\boldsymbol{v}})(1+\boldsymbol{e}_{\boldsymbol{v}}\boldsymbol{e}_{\boldsymbol{v}}')\delta(\epsilon\boldsymbol{e}_{\boldsymbol{v}} - \epsilon'\boldsymbol{e}_{\boldsymbol{v}}' + v\boldsymbol{q}). \tag{B12}$$

The two-dimensional delta function in the latter integral fixes both $\boldsymbol{e_v}$ and $\boldsymbol{e'_v}$. We substitute $\boldsymbol{q}$ from the argument of the delta function into the rest of the integrand and then average the delta function over directions of $\boldsymbol{q}$. After such an averaging the integrand depends only on the angle ϕ between $\boldsymbol{e_v}$ and $\boldsymbol{e'_v}$.

$$J(\epsilon,\epsilon',q)=\int\frac{d\phi}{v^2q}\left[\tau'\epsilon'+\tau\epsilon-(\tau'\epsilon+\tau\epsilon')\cos\phi\right](1+\cos\phi)\delta\left(\sqrt{\epsilon^2+\epsilon'^2-2\epsilon\epsilon'\cos\phi}-vq\right)=\tilde{J}(\epsilon,\epsilon',q)+\tilde{J}(\epsilon',\epsilon,q), \tag{B13a}$$

$$\tilde{J}(\epsilon,\epsilon',q)=\tau(\epsilon)\frac{v^2q^2+\epsilon^2-\epsilon'^2}{v\epsilon^2\epsilon'}\sqrt{\frac{(\epsilon+\epsilon')^2-v^2q^2}{v^2q^2-(\epsilon-\epsilon')^2}}. \tag{B13b}$$

This result should be treated as zero if the argument of the square root is negative [this fact was previously expressed in terms of the additional factor $\theta_0(\epsilon,\omega,q)$]. Taking advantage of the symmetry of Eq. (B13), we recast $\mathbf{\Gamma}$ in the form of Eqs. (12) and (14). In particular, we identify the function (B13) with Eq. (14) as

$$\boldsymbol{\gamma}(\epsilon,\omega,q)=-N\frac{\boldsymbol{q}}{2q^2}\,|\epsilon(\epsilon+\omega)|\tilde{J}(\epsilon,\epsilon+\omega,q),$$

where we have multiplied the result by N to account for the spin and valley degeneracy. Note, that in this Appendix τ stands for the transport scattering time, unlike Eq. (14), where τ is just the mean free time. In graphene these two quantities differ by a factor of two[22].

Appendix C: Polarization operator in graphene

In the basis of exact eigenstates we can use the standard expression for the polarization operator, including the vertices $\lambda^{\nu,\nu'}_{\mathbf{k},\mathbf{k}'}$ and summing over the two bands:

$$\Pi^R(\omega,\boldsymbol{q})=-4\sum_{\nu\nu'}\int\frac{d^2k}{(2\pi)^2}|\lambda^{\nu,\nu'}_{\boldsymbol{k},\boldsymbol{k}+\boldsymbol{q}}|^2\frac{n_F(\boldsymbol{k})-n_F(\boldsymbol{k}+\boldsymbol{q})}{\omega-E_\nu(\boldsymbol{k}+\boldsymbol{q})+E_{\nu'}(\boldsymbol{k})+i\eta} \tag{C1}$$

[the prefactor of 4 is due to spin and valley degeneracy; the overall sign is chosen in such a way that the static polarization operator at $q=0$ yields the density of states (63)]. Here $n_F(\boldsymbol{k})$ stands for the Fermi distribution.

The polarization operator was calculated in detail in Ref. 14. Nevertheless, we will add some details in order to make the paper self-contained. The complete expression for the polarization operator might also be useful for numerical computations.

In order to simplify the expression for the polarization operator we multiply Eq. (C1) by the integral of a δ-function, which is unity:

$$\Pi^R=-4\sum_{\nu\nu'}\int\frac{d^2k}{(2\pi)^2}|\lambda^{\nu,\nu'}_{\boldsymbol{k},\boldsymbol{k}+\boldsymbol{q}}|^2\frac{[n_F(\boldsymbol{k})-n_F(\boldsymbol{k}+\boldsymbol{q})]}{\omega-E_\nu(\boldsymbol{k}+\boldsymbol{q})+E_{\nu'}(\boldsymbol{k})+i\eta}\int d\epsilon_1\delta\left(\epsilon_1-E_{\nu'}(\boldsymbol{k})\right)\int d\epsilon_2\delta\left(\epsilon_2-E_\nu(\boldsymbol{k}+\boldsymbol{q})\right). \tag{C2}$$

Now we can use the δ-functions to express the integrand in Eq. (C1) in terms of ϵ_i. After that the momentum integral will only contain the two δ-functions and can be evaluated analytically similarly to how it was done in Appendix A for the non-linear susceptibility. Then the polarization operator takes the form

$$\Pi^R=-\int\frac{d\epsilon_1 d\epsilon_2}{\epsilon_1\epsilon_2}[n_F(\epsilon_1)-n_F(\epsilon_2)]\frac{(\epsilon_1+\epsilon_2)^2-v^2q^2}{\omega-\epsilon_2+\epsilon_1+i\eta}F(\epsilon_1,\epsilon_2), \tag{C3}$$

where

$$F(\epsilon_1,\epsilon_2)=\sum_{\nu\nu'}\int\frac{d^2k}{(2\pi)^2}\delta\left(\epsilon_1-\nu'vk\right)\delta\left(\epsilon_2-\nu v|\boldsymbol{k}+\boldsymbol{q}|\right). \tag{C4}$$

The calculation of this function can be performed along the lines of Appendix A. The result is

$$F(\epsilon_1,\epsilon_2)=\frac{\epsilon_1|\epsilon_2|}{\pi^2v^2}\frac{1}{\sqrt{[(\epsilon_1+vq)^2-\epsilon_2^2]\,[\epsilon_2^2-(\epsilon_1-vq)^2]}}\,\Theta(\epsilon_1,\epsilon_2), \tag{C5}$$

where

$$\Theta(\epsilon_1,\epsilon_2)=\theta(\epsilon_1>0)\theta\left[(\epsilon_1-vq)^2<\epsilon_2^2<(\epsilon_1+vq)^2\right]-\theta(\epsilon_1<0)\theta\left[(\epsilon_1+vq)^2<\epsilon_2^2<(\epsilon_1-vq)^2\right]. \tag{C6}$$

The θ-functions are the result of imposing the condition that the cosine of the angle between the two momenta in Eq. (A13) is less than unity. In other words, the expression under the square root in Eq. (C5) has to be positive (and thus $F(\epsilon_1,\epsilon_2)$ is a real function).

The resulting expression can be simplified by the series of simple transformations: (i) change the sign of ϵ_i in the second term in Eq. (C6); (ii) resolve the θ-functions in order to identify the integration limits; (iii) introduce the sum and difference

$$z_1=\epsilon_1+\epsilon_2,\quad z_2=\epsilon_1-\epsilon_2,$$

(iv) introduce the dimensionless variables

$$Q=\frac{q}{2T},\quad W=\frac{\omega}{2T},\quad x=\frac{\mu}{T}.$$

As a result we arrive at the following expression

$$\Pi^R=\frac{q}{4\pi^2 v}\int\limits_0^1\int\limits_0^1\frac{dz_1dz_2}{z_1\sqrt{(1-z_1^2)(1-z_2^2)}}\left[(z_1^{-2}-1)\left(\frac{Q}{z_2Q+W+i\eta}+\frac{Q}{z_2Q-W-i\eta}\right)J_1(z_1^{-1},z_2,x_i)\right. \tag{C7}$$

$$\left.+(1-z_2^2)\left(\frac{Q}{z_1^{-1}Q+W+i\eta}+\frac{Q}{z_1^{-1}Q-W-i\eta}\right)J_2(z_1^{-1},z_2,x_i)\right]$$

$$J_{1(2)}(z_1,z_2,x)=\tanh\frac{(z_1+z_2)Q+x}{2}+\tanh\frac{(z_1+z_2)Q-x}{2}\mp\tanh\frac{(z_1-z_2)Q+x}{2}\mp\tanh\frac{(z_1-z_2)Q-x}{2} \tag{C8}$$

In particular, it is instructive to further simplify the imaginary part of the polarization operator:

$$\mathrm{Im}\Pi^R(\omega,\boldsymbol{q})=\frac{q}{4\pi v}\left[\theta(|W|>Q)P_1(W,Q)+\theta(|W|<Q)P_2(W,Q)\right]; \tag{C9a}$$

$$P_1(W,Q)=\frac{\mathrm{sgn}W}{\sqrt{W^2/Q^2-1}}\int\limits_0^1 dz\sqrt{1-z^2}\;I_1(z;Q,W,x); \tag{C9b}$$

$$P_2(W,Q)=\theta(|W|<Q)\frac{\mathrm{sgn}W}{\sqrt{1-W^2/Q^2}}\int\limits_1^\infty dz\sqrt{z^2-1}\;I_1(z;Q,W,x); \tag{C9c}$$

$$I_1(z;Q,W,x)=\tanh\frac{zQ+W+x}{2}+\tanh\frac{zQ+W-x}{2}-\tanh\frac{zQ-W-x}{2}-\tanh\frac{zQ-W+x}{2}. \tag{C9d}$$

Comparing Eqs. (C9) and (16) we conclude, that despite clear similarity, these expression are *not* proportional to each other. Therefore the proportionality between the non-linear susceptibility and the imaginary part of the polarization operator mentioned in Ref. 3 is not a general theorem, but rather a property of the limiting cases considered in Ref. 3.

Having the full expression for the polarization operator it is straightforward to derive the well-known expressions:

$$\Pi^R(\mu=\omega=0;T\ll vq)\approx q/4v, \tag{C10}$$

$$\Pi^R(\mu=\omega=0;T\gg vq)\approx 4T\ln 2/(\pi v^2), \tag{C11}$$

$$\Pi^R(q\ll k_F;\omega=T=0)\approx 2k_F/\pi v, \tag{C12}$$

$$\mathrm{Re}\Pi^R(q\ll k_F;T=0)\approx\frac{2k_F}{\pi v}\left[1-\frac{|\omega|\theta(\omega^2>v^2q^2)}{\sqrt{|\omega|-vq}}\right],\qquad \mathrm{Im}\Pi^R(q\ll k_F;T=0)\approx\frac{2k_F}{\pi v}\frac{\omega\;\theta(|\omega|<vq)}{\sqrt{v^2q^2-\omega^2}}. \tag{C13}$$

Appendix D: Numerical evaluation of the drag coefficient

In this Appendix we show the results of the numerical evaluation of the drag coefficient using Eqs. (1), (7), and (19). The interaction propagator (9) was calculated using the polarization operator calculated in Appendix C in the absence of disorder, see Eq. (C7). The non-linear susceptibility was evaluated using Eqs. (16). The particle density was found from Eq. (65). The particular values of the inter-layer spacing d, temperature T, and the interaction parameter α were chosen to resemble possible realizations of the drag measurement in graphene-based devices[9,39].

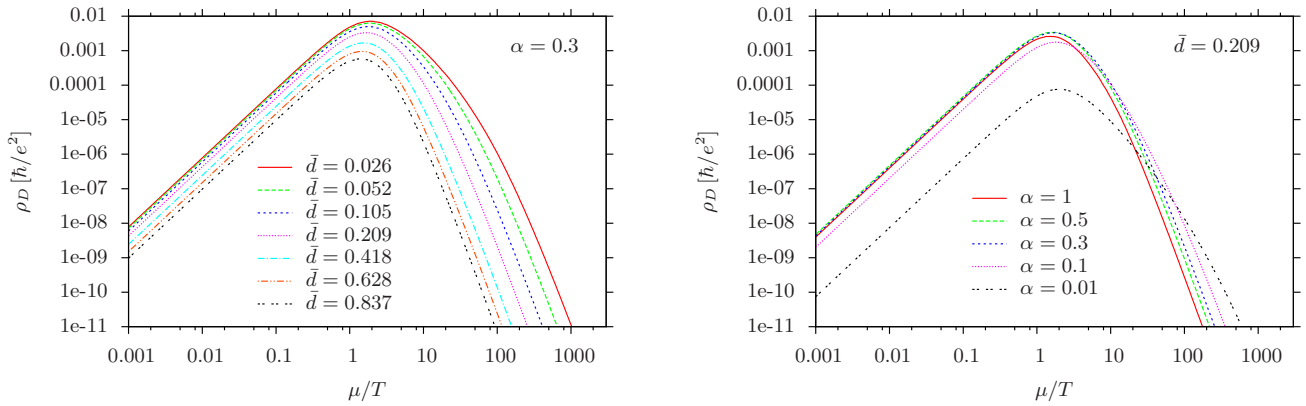

FIG. 7: Numerical estimate of the drag resistance. The left panel shows $\rho_D(\mu/T)$ for $\alpha = 0.3$ (see Ref.25) and various values of d (see Table II). The right panel shows $\rho_D(\mu/T)$ for $\bar{d} = 2Td/v$ and various values of α.

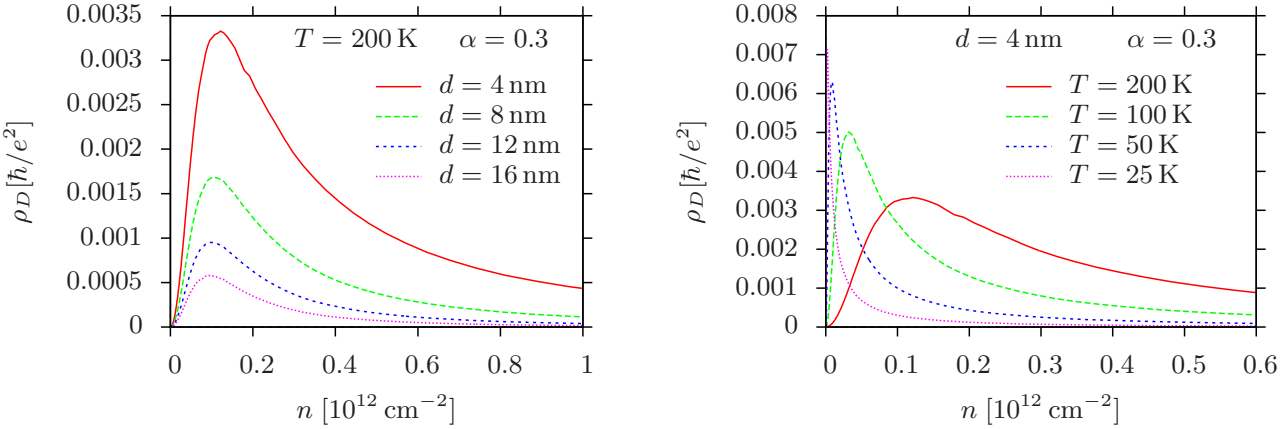

FIG. 8: The data from Fig. 7 in the linear scale. The chemical potential is converted to the carrier density, n, using Eq. (65).

TABLE II: Values of the dimensionless parameter $\bar{d} = 2Td/\hbar v$ for different inter-layer separations d and temperatures T.

T	$d = 4\,\mathrm{nm}$	6 nm	8 nm	12 nm	16 nm	18 nm
25 K	0.026	0.039	0.052	0.078	0.105	0.118
50 K	0.052	0.078	0.105	0.157	0.209	0.235
100 K	0.105	0.157	0.209	0.314	0.418	0.471
200 K	0.209	0.314	0.418	0.628	0.837	0.942

The maximal values of ρ_D are apparently reached for $\alpha \sim 0.5$. The drag resistance at the peak is a non-monotonous function of α, since we are calculating the drag conductivity within the lowest-order perturbation theory, but still keep $\alpha \neq 0$ in the denominator of the interaction propagator in order to describe screening effects. The peak values of ρ_D are achieved for carrier densities such that $\mu \sim T$ (only weakly depending on d).

[1] B.L. Altshuler and A.G. Aronov, in *Electron-Electron Interactions in Disordered Systems*, eds. A.L. Efros, M. Pollak (North-Holland, Amsterdam, 1985).

[2] A.G. Rojo, J. Phys.: Condens. Matter, **11** R31 (1999).

[3] A. Kamenev and Y. Oreg, Phys. Rev. B **52**, 7516 (1995).

[4] K. Flensberg, B.Y.-K. Hu, A.-P. Jauho, and J.M. Kinaret, Phys. Rev. B **52**, 14761 (1995).

[5] B.N. Narozhny, I.L. Aleiner, and A. Stern, Phys. Rev. Lett. **86**, 3610 (2001); F. von Oppen, S.H. Simon, and A. Stern, Phys. Rev. Lett. **87**, 106803 (2001).

[6] I.V. Gornyi, A.D. Mirlin, and F. von Oppen, unpublished.

[7] A.-P. Jauho and H. Smith, Phys. Rev. B, **47** 4420 (1993);

[8] K. Flensberg and B.Y.-K. Hu, Phys. Rev. Lett., **73**, 3572 (1994); Phys. Rev. B, **52** 14796 (1995).

[9] S. Kim, I. Jo, J. Nah, Z. Yao, S.K. Banerjee, and E. Tutuc, Phys. Rev. B **83**, 161401(R) (2011).

[10] P.M. Solomon, P.J. Price, D.J. Frank, and D.C. La Tulipe, Phys. Rev. Lett. **63**, 2508 (1989); T.J. Gramila, J.P. Eisenstein, A.H. MacDonald, L.N. Pfeiffer, and K.W. West, Phys. Rev. Lett. **66**, 1216 (1991).

[11] A.B. Kashuba, Phys. Rev. B **78**, 085415 (2008).

[12] L. Fritz, J. Schmalian, M. Müller, and S. Sachdev, Phys. Rev. B **78**, 085416 (2008); M. Müller, J. Schmalian, and L. Fritz, Phys. Rev. Lett. **103**, 025301 (2009).

[13] M.S. Foster and I.L. Aleiner, Phys. Rev. B **79**, 085415 (2009).

[14] M. Schütt, P.M. Ostrovsky, I.V. Gornyi, A.D. Mirlin, Phys. Rev. B **83**, 155441 (2011).

[15] M. Schütt, P.M. Ostrovsky, I.V. Gornyi, M. Titov, B.N. Narozhny, and A.D. Mirlin, in preparation.

[16] A. Stern and B.I. Halperin, Phys. Rev. B **52**, 5890 (1995).

[17] I.V. Gornyi, A.D. Mirlin, and F. von Oppen, Phys. Rev. B **70**, 245302 (2004).

[18] The non-linear susceptibility in graphene was previously evaluated in Refs. 19 and 20 under the assumption that the Fermi energy is the largest energy scale in the problem. Then the relevant frequencies (of order $T \ll E_F$) and momenta ($q \ll k_F$) are small and $\mathbf{\Gamma}$ can be expressed in terms of a power series in ω/E_F and q/k_F. In Ref. 19 it was found that in the leading order the non-linear susceptibility vanishes, while the subleading term was discarded in favor of the contribution due to the trigonal warping. In contrast Ref. 20 focused on the subleading term, which turned out to be identical to the Fermi-liquid expression[3].

[19] B.N. Narozhny, Phys. Rev. B **76**, 153409 (2007).

[20] W. Tse, Ben Yu-Kaang Hu, and S. Das Sarma, Phys. Rev. B **76**, 081401 (2007).

[21] Expressing the electron-hole asymmetry as a derivative of the single-layer conductivity with respect to the chemical potential[5], one might conclude[19] that for the case of short-ranged disorder (where σ_i is independent of μ_i or carrier density[22]) the drag should vanish. However, the non-linear susceptibility in ballistic regime contains another term, which is proportional[6] to $\partial\tau/\partial\mu$. Hence there is no accidental cancellation of the drag and we can conclude that taking into account energy dependence of the scattering time does not lead to qualitative changes in the theory.

[22] E. McCann, K. Kechedzhi, V.I. Falko, H. Suzuura, T. Ando, and B. L. Altshuler, Phys. Rev. Lett. **97**, 146805 (2006).

[23] For $\mu \gg T$ the drag conductivity is largely determined by $vq \gg \omega \sim T \gg \tau^{-1}$. In turn, the non-linear susceptibility is determined by $\epsilon \sim T \gg \tau^{-1}$. Thus we can use the theory developed in Appendix A, even though technically we can only represent the Green's function by Eq. (A10) for $\epsilon \gg \tau^{-1}$. Moreover, in the region $vq, \omega \ll \tau^{-1}$ we should take into account multiple impurity scattering, i.e. dress the non-linear susceptibility by diffusons. In the ballistic regime, however, the region $vq, \omega \ll \tau^{-1}$ is irrelevant.

[24] M.I Katsnelson, Phys. Rev. B **84**, 041407 (2011).

[25] N.M.R. Peres, J.M.B. Lopes dos Santos, and A.H. Castro Neto, EuroPhys. Lett., **95** 18001 (2011).

[26] T. Ando, J. Phys. Soc. Jpn. **75**, 074716 (2006); K. Nomura and A.H. MacDonald, Phys. Rev. Lett. **96**, 256602 (2006); *ibid.* **98**, 076602 (2007).

[27] V.V. Cheianov and V.I. Falko, Phys. Rev. Lett. **97**, 226801 (2006).

[28] P.M. Ostrovsky, I.V. Gornyi, and A.D. Mirlin, Phys. Rev. B **74**, 235443 (2006).

[29] N.H. Shon and T. Ando, J. Phys. Soc. Jpn. **67**, 2421 (1998).

[30] I. L. Aleiner and K. B. Efetov, Phys. Rev. Lett. **97**, 236801 (2006).

[31] K. Kechedzhi, O. Kashuba, and V.I. Falko, Phys. Rev. B **77** 193403, (2008).

[32] G. Zala, B.N. Narozhny, and I.L. Aleiner, Phys. Rev. B **64**, 214204 (2001).

[33] A.A. Abrikosov and S.D. Beneslavskii, Sov. Phys. JETP **32**, 699 (1971); J. Gonzalez, F. Guinea, and M.A.H. Vozmediano, Phys. Rev. B **59**, R2474 (1999); D.T. Son, *ibid.* **75**, 235423 (2007).

[34] J. Gonzalez, F. Guinea, and M.A.H. Vozmediano, Nucl. Phys. B **424**, 596 (1994).

[35] D.E. Sheehy and J. Schmalian, Phys. Rev. Lett. **99**, 226803 (2007).

[36] M.S. Foster and I.L. Aleiner, Phys. Rev. B **77**, 195413 (2008).

[37] K.S. Novoselov, A.K. Geim, S.V. Morozov, D. Jiang, M.I. Katsnelson, I.V. Grigorieva, S.V. Dubonos, and A.A. Firsov, Nature **438**, 197 (2005).

[38] Y. Zheng and T. Ando, Phys. Rev. B **65**, 245420 (2002).

[39] A.K. Geim, K.S. Novoselov, and L. Ponomarenko, private communication.

[40] A.A.Kozikov, A.K. Savchenko, B.N. Narozhny, and A.V. Shytov, Phys. Rev. B **82**, 075424 (2010).

[41] J.P. Reed, B. Uchoa, Y.I. Joe, Y. Gan, D. Casa, E. Fradkin, and P. Abbamonte, Science **330**, 805 (2010).

[42] T. Ando, T. Nakanishi, and R. Saito, J. Phys. Soc. Jpn. **67**, 2857 (1998).